3D printed Shear force sensors

S. (Sayedamid) Zia

BSc Report

Committee:
Prof.dr.ir. G.J.M. Krijnen
G.J.W. Wolterink, MSc
Ing. R.G.P. Sanders
Dr.ir. R.A.R. van der Zee

February 2019

006RAM2019
Robotics and Mechatronics
EE-Math-CS
University of Twente
P.O. Box 217
7500 AE Enschede
The Netherlands

Abstract

Easily manufacturing of sensors with little waste and manufacturing costs is often desired in many fields, an example is the field of rehabilitation engineering. There is a way of manufacturing that can fulfil these needs called Additive Manufacturing (AM) and more specific 3D-printing. This research will delve into seeing if it is possible to design and create a 3D-printed shear force sensor using carbon doped thermoplastics.

There are many designs that can be approached but this research will be focused on a three layer design and cylindrical design. The three layer design consists of two layers of conductive filament called ETPU separated by beams of flexible filament called x60. The cylindrical design consists of two half cylinders with different radii consisting of ETPU with beams of x60 between them.

A model will be determined which takes the normal force, shear force and fringing effect into account. The measurement setup includes separately designed tools that are 3D-printed out of an ABS plastic filament. The range of shear force will be between zero and twelve Newton for both the model and the measurement.

There were multiple discrepancies between the model and the measurements for the three layer design which were most likely caused by the small size of the sensor making the dimensions of the sensor harder to accurately determine. The cylindrical design deformed when a shear force was applied due to its flexibility. This caused it to behave differently than expected in the model. This made the model unusable with this type of cylindrical sensor consisting of the flexible materials.

It was possible to measure shear force using capacitive readout with the three layered design for forces ranging from two to twelve Newtons. However, a stable normal force acting on the sensor is needed for it to work properly.

Acknowledgements

I would like to take a moment and show my gratitude to everyone who has aided me during this research assignment. An incredible amount of gratitude goes towards my committee and the members of NIFTy, who have given assistance by means of weekly meetings and sharing helpful thoughts and information. I would like to express my thanks to Gijs Krijnen who offered me this assignment and has steered me in the right direction whenever I needed it. My utmost appreciation goes to my daily supervisor and member of my committee, Gerjan Wolterink. He has helped me tremendously with tips and tricks regarding the 3D-printer, the measurement equipment and this report. I appreciate his help very much and I could not have wished for a better supervisor.

Contents

Chapter 1

Introduction

Thin, easily manufactured and wearable shear force sensors have been desired in the field of rehabilitation engineering for some time. To start off with an example, imagine a patient who suffered a stroke and cannot exert as much force in his fingers as he used to. To properly support the patient and give the exact help he needs, numerous types of data have to be known such as the normal force and shear force that the patient can exert. Knowing these forces, the physical therapist can adjust his care, and might be able to aid the patient more than he would without the sensing.

To create these sensors, a way of manufacturing called Additive Manufacturing (AM) can be applied. 3D-printing is a type of Additive Manufacturing which can create a large variety of products with little waste and great freedom of design.

A common type of manufacturing is substractive manufacturing. Where the way to manufacture is by chipping away on a certain material until the product is created, including the waste from manufacturing it.

The advantages of 3D-printing over traditional manufacturing entail its ability to produce products in small series at a low cost, meaning a prototype can be designed and the cost of manufacturing one item stays the same no matter the quantity. So for small quantities it is cheaper than traditional production.

3D-printing is more customisable and adaptable to a variety of situations. There is an almost unlimited number of changes that can be made to a designed product to suit the designers needs. Even if the customisation makes the product more complex, this does not affect the price of production as drastically as for traditional manufacturing. [1].

Currently, research is done on creating reliable 3D-printed sensors. There are already multiple examples of 3D-printed sensors as seen in Welleweerd et al. [2], Perez et al. [3], Tichelaar et al. [4] and Eijking et al. [5]. However, the boundaries have to be pushed further to get a better understanding of 3D-printed sensors and find more applications for these type of sensors

1.1 Problem statement

Shear force sensors have been made before with electrode-patterned polymer films, strain gauges etc. which will be touched upon in 1.3. 3D-printing could offer many benefits if used to create a shear force sensor, because it is relatively easy and a fast manufacturing method. Materials are easy to come by and a 3D-printer can print products as thin as the nozzle on the printer can extrude. However, the use of 3D-printing is scarcely studied and there is much to learn. It is therefore important to explore the uses of this way of manufacturing to get more insight on its properties, potential and limitations.

1.2 Goals

This research will be concentrated on shear force sensors, manufactured with 3D-printing using conductive carbon doped thermoplastic polyurethane (ETPU) and a flexible filament. This research will examine the following:

- Can 3D-printed structures, consisting of carbon doped thermoplastics, be used for sensing shear forces?
- Can this be done in a form and size hat would allow the use in sensing the interaction forces in human grasps?

This research will not delve into different filament choices and other methods of 3D-printing due to constraints.

1.3 Literature study

While examining the literature regarding shear force sensing and 3D-printed sensors overall, multiple ideas have been formed regarding what is possible to create and mimic from other sensors to design a fully functioning, thin and easy to manufacture shear force sensor.

1.3.1 Strain gauge

Multiple 3D-printed sensors based on strain-sensing have already been designed and tested by Welleweerd et al. [2], Perez et al. [3] and Tichelaar et al. [4]. Using a method where they measure the resistance of the strain gauge and depending on the force applied to the gauge, it would stretch or compress and change in resistance.

1.3.2 Capacitive Three Layer structure

The design for a normal force sensor made by Wolterink et al. [6] showed two layers of ETPU on top of each other which had a high interlayer impedance. This resulted in an effect where the layers of ETPU acted like a capacitor and a

capacitance could be measured. The normal force would push the layers closer to each other which increased the capacitance and this could be read out.

It could be possible to apply a shear force to this type of sensor and see the change in capacitance caused by less overlap of the layers and decrease of the distance between both the layers. The sensor would be thin and easy to manufacture. However, it would be difficult to accurately distinguish the normal- from the shear-force.

Fringing Effect

The largest difficulty in this type of sensor lays in the effects of fringing. When there is no overlap, a capacitance can still be measured, this is caused by the fringing effect. In Figure 1.1 the fringing effect can be seen at the edges of plates. If the plates would have zero overlap, the fringing would still occur resulting in a capacitance which does not show drastic change when the plates would move sideways. However, if the distance between the plates would change this could still have a considerable effect.

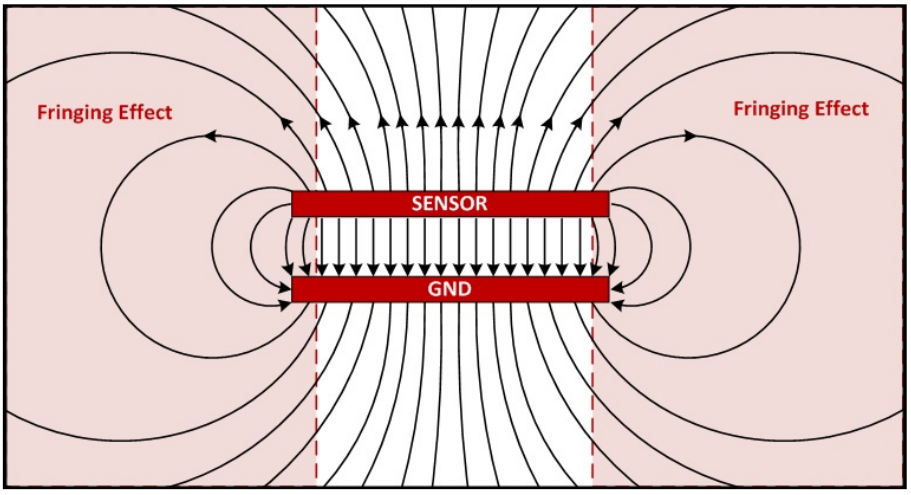

Figure 1.1: Fringing effect shown at the edges of two parrallel plates [7].

1.3.3 Capacitive Wire structure

At first designed for a different purpose, Shemelya et al. [8] had designed a shear force sensor to be used in a satellite. The structure consisted of two surfaces with embedded conductive wires, the surfaces were on top of each other without the wires overlapping as shown in Figure 1.2. If a shear force were to be applied, the wires would move causing a change in overlap and in turn a a change in capacitance. This could then be related to the shear force.

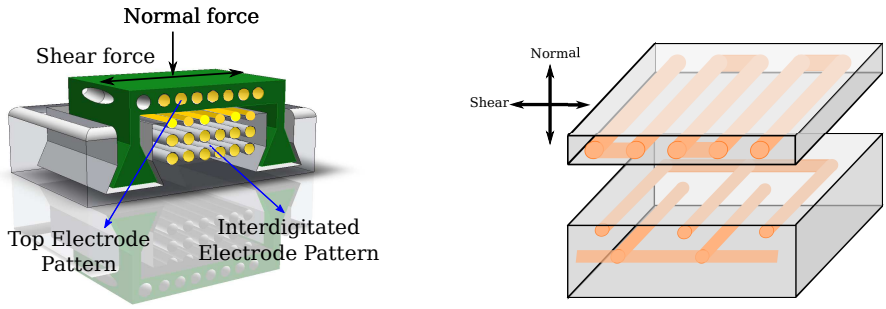

Figure 1.2: Capacitive structure where the capacitance changes when a shear force is applied [8].

1.3.4 Capacitive Sheet type structure

A different approach unrelated to 3D-printing is given by Shigeru et al. [9] where the shear force sensor consists of two electrode patterned polymer films with an elastic rubber ring between them which is filled with a liquid electrolyte. When a shear force is applied, the patterned films mutually move which changes the distance between the internal electrodes of the sensor. This causes a change in current between the electrodes which can be measured. By monitoring the current, the shear force can be determined. If the sensor contains multiple electrodes, it is possible to measure two-dimensional shear force and normal force. In Figure 1.3 a cut out of the sensor and its working principle is shown, when a shear force is applied to the top surface.

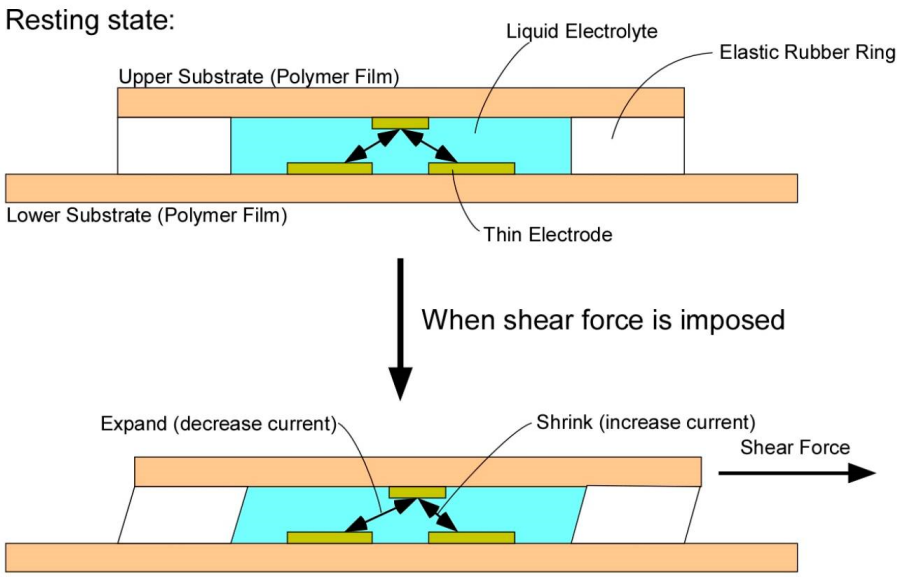

Figure 1.3: Two sheets of electrode patterned polymer films with a rubber ring and a liquid electrolyte between them. A change in shear force causes a change in current between the electrodes [9].

Chapter 2

Designs

When considering the literature regarding shear force sensing, multiple design ideas can be formed to create a shear force sensor which can be 3D-printed. These design ideas will be touched upon and the most viable options will be further analyzed.

2.1 Strain-gauge

One of the first options that seemed easy to implement is the application of strain gauges which would stretch or compress when a shear force is applied to them. However, the size and implementation seemed difficult. For the strain gauge to be sufficiently sensitive to small changes, it would have to be of a larger size than desired. To have a strain gauge of the desired size would cause a smaller change in resistance and a smaller mean resistance.

2.2 Capacitive Three layer structure

A variant of this type of sensor would be two layers of ETPU seperated by a layer of flexible material making it a Three layer structure. However, if the resulting flexibility is not sufficient, the flexible layer can be seperated into thinner parts which are more flexible and will cause a bigger change in the overlapping area of the ETPU layers. An example can be found in Figure 2.1.

2.3 Capacitive Wire structure

This same structure could be built the same way, in a smaller size, where the wires are the size of the strands that are extruded by the 3D-printer. To give a better understanding refer to Figure 2.2. The lines of ETPU will have some change overlap when a shear force is applied which results in a change of capac-

Figure 2.1: Capacitive structure where the capacitance increases when a shear force is applied. Flexibility in this sensor is higher because of the thinner flexible "walls" seperating the ETPU.

itance. If it is possible to determine the change in capacitance caused by the shear force, it would be possible to determine the applied shear force.

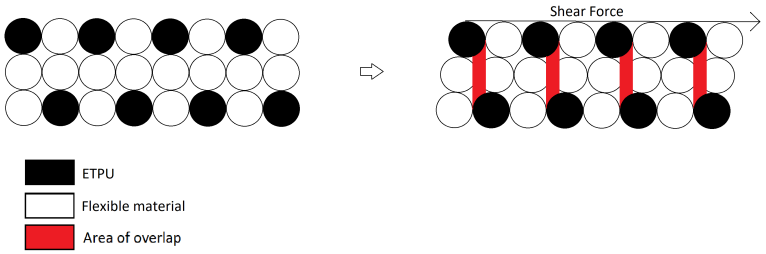

Figure 2.2: Same concept as structure shown in Figure 1.2. However, it is on a much smaller scale. One circle is one line of TPU/ETPU extruded by the 3D-printer. The change in capacitance between the left picture and the right picture caused by increased overlap from the shear force, could be an indicator for the amount of shear force applied. At least one of the top structures should have two independent electrode structures to make a simultaneous sum and difference measurement possible to determine both normal and shear forces.

However, the effects of fringing will make the change in capacitance from the overlap practically invisible which will make the sensor much less accurate and sensitive.

2.4 Capacitive Sheet type structure

The same type of sensor as shown in Figure 1.3 can be applied in a 3D-printed design. However, from a practicality perspective, it should not contain liquids. The design can be seen in Figure 2.3. It applies the same concept as shown in Figure 1.3, but instead of measuring the current, the capacitance change is measured between the ETPU parts. This makes it also possible to have two degrees of freedom (2-DoF) by measuring from both ETPU parts on the lower layer. However, as mentioned in 1.3.2 fringing will cause the sensor to still have a capacitance and the rate of change of the capacitance could be too small to result in an accurate readout.

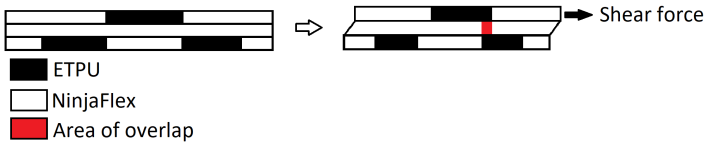

Figure 2.3: Three layers of flexible material where the top and bottom layer have ETPU incorporated in them having the same function as the electrodes in Figure 1.3. The change in capacitance caused by the applied shear force can be measured and correlated to the applied shear force. However, fringing could make the amount of change in capacitance relatively small, making the sensor less sensitive than desired.

2.5 Capacitive Dome structure

A different type of approach is the dome structure as shown in Figure 2.4.

The way this structure will measure the shear force is by measuring the capacitance between the outer- and inner domes. When a shear force is applied to the outer dome, the flexible material inside the dome will stretch and compress, changing the distance between the inner- and outer domes which causes a change in capacitance.

If the inner dome were to be separated by a layer of non-conductive material, the change in capacitance could be measured in 2-DOF or 4-DOF if the inner dome were to be separated into four. However, this could make the capacitance much smaller and therefore harder to measure.

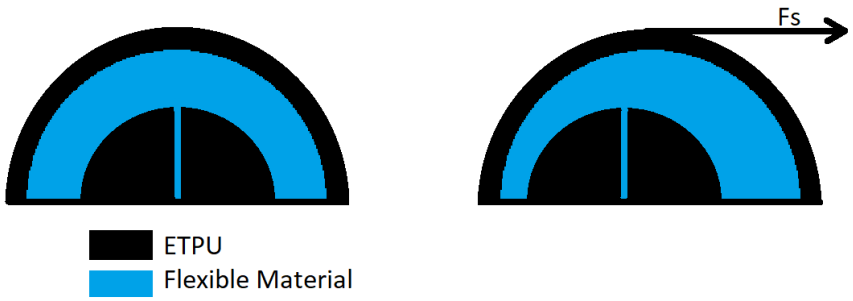

Figure 2.4: Capacitive sensor in the shape of a dome which can be used for 2-DOF or 4-DOF shear force sensing

2.6 Final design

Determining the most suitable design for this research depends on multiple factors. The designs mentioned in 2.1, 2.3 and 2.4 will not be considered for this research. The strain gauge at the desired size would be too inaccurate and insensitive and for the capacitive sensors mentioned the effects of fringing would have a severe effect on the accuracy and sensitivity of the capacitive sensors and are therefore also unsuitable.

The Capacitive three layer structure described in 2.2 and the Capacitive Dome structure described in 2.5 can be considered. Of course, these types of sensors will still be affected by the fringing effect. However, the effect can be minimized by increasing the size and decreasing the distance between the layers and it can be taken into account when creating the model.

Chapter 3

Analysis

To determine the expected behaviour of the designs chosen in 2.6, it is necessary to determine the model of these designs. The models will give insights in what kind of capacitances and what kind of changes to the capacitance caused by the shear force can be expected. The models will be determined separately for both sensors.

3.1 Model

3.1.1 Three Layer structure

There are multiple factors that have to be determined to design an accurate model of the three layer structure, consisting of two layers of conductive TPU and a flexible layer. For the three layered structure, the effects of normal force will be determined first. Thereafter the effects of the shear force will be considered and finally the capacitance will be determined including the effects of fringing.

Normal Force

The normal force does affect the material and it has to be taken into account. Using the Young's modulus (E) and Poisson's ratio (ν), it is possible to determine the effect of Normal force. The Poisson's ratio for TPU based materials was determined to be between 0.48 0.5 by Qi et al. [10]. It is assumed to be 0.5. A_{N} is the area on which the normal force is exerted.

ΔL is the change in size parallel to the exerted force, $\Delta L'$ is the change in size perpendicular to the exerted force. Figure 3.1 shows both these in an example scenario where a force is exerted on a cube. This same principle is applied to the example of the three layer structure resulting in the effects illustrated in Figure 3.2.

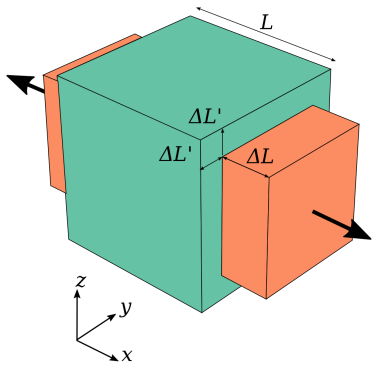

Figure 3.1: A cube which experiences a force, causing expansion or contraction in different direction [11].

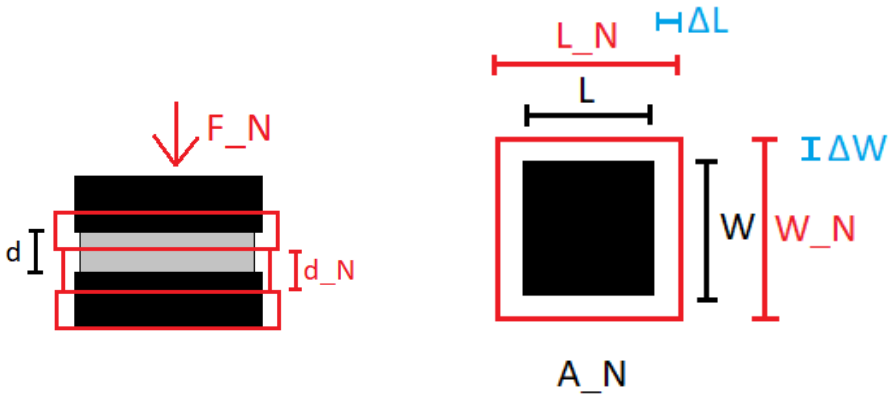

(a) Side view of the Three layer structure. Red illustration is the result of a normal force F_{N} applied to the original black and gray structure.

(b) Top view of the Three layer structure. Red illustration is the result of a normal force F_{N} applied to the original black area A_{N}

Figure 3.2: Three layer structure experiencing a normal force

$$\nu = -\frac{\Delta L'}{\Delta L} \tag{3.1}$$

$$0.5 = -\frac{\Delta L'}{\Delta L} \tag{3.2}$$

$$\Delta L = -2\Delta L' \tag{3.3}$$

$$E = \frac{F_{\mathrm{N}} L_0}{A_{\mathrm{N}} \Delta L} \tag{3.4}$$

$$\Delta L = \frac{F_{\mathrm{N}} L_0}{A_{\mathrm{N}} * E} \tag{3.5}$$

$$L_{\mathrm{N}} = L + 2\Delta L' \tag{3.6}$$

$$L_{\mathrm{N}} = L + \Delta L \tag{3.7}$$

If a normal force (F_{N}) is exerted, most of the deformation will happen to the most flexible material, the material between the plates. The change in its length, width and height can then be determined as follows.

$$L_{\mathrm{N}} = L + \frac{F_{\mathrm{N}} L}{A_{\mathrm{N}} E} = (1 + \frac{F_{\mathrm{N}}}{A_{\mathrm{N}} E})L \tag{3.8}$$

$$W_{\mathrm{N}} = W + 2\Delta W' = W + \Delta W = (1 + \frac{F_{\mathrm{N}}}{A_{\mathrm{N}} E})W \tag{3.9}$$

$$d_{\mathrm{N}} = d - 2\Delta d = (1 - \frac{2F_{\mathrm{N}}}{A_{\mathrm{N}} E})d \tag{3.10}$$

W is the width of the area $A_{\mathrm{N}} = WL$ which experiences the normal force F_{N}, d is the distance between the plates.

Plate movement

The effects of shear force on the three layer structure can be approached by observing the movement of the upper layer. The effect can be seen in the illustration shown in Figure 3.3.

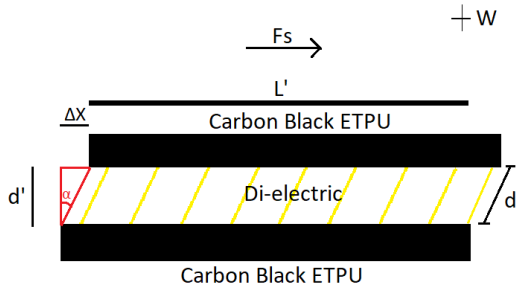

Figure 3.3: The effect of shear force on the three layer structure.

The horizontal plate movement, Δx in Figure 3.3, can be determined using the shear modulus. The shear modulus is defined as

$$G = \frac{F_{\mathrm{s}} d'_{\mathrm{N}}}{\Delta x A_{\mathrm{s}}} \tag{3.11}$$

Where A_s is the area on which the shear force is exerted on.

This can be rewritten to

$$\Delta x = \frac{F_s d'_N}{G A_s} \tag{3.12}$$

The dielectric is assumed to be a stiff beam because the larger width compared to the height of the dielectric. This would make it behave approximately more like a stiff beam. Therefore it can be assumed that the angle between Δx and d' is 90° as shown in Figure 3.3. Knowing this it is possible to express the unknown parameter d' differently and rewriting equation 3.12, making the equation only depend on one variable F_s. Where d is the distance between the plates without forces acting on the structure, also described in Figure 3.3.

$$d_N^2 = {d'_N}^2 + \Delta x^2 \tag{3.13}$$

$$d'_N = \sqrt{d_N^2 - \Delta x^2} \tag{3.14}$$

$$\Delta x = \frac{F_s \sqrt{d_N^2 - \Delta x^2}}{G A_s} \tag{3.15}$$

$$\Delta x = \frac{F_s d_N}{G A_s \sqrt{1 + (\frac{F_s}{G A_s})^2}} \tag{3.16}$$

This does mean that for $F_s \gg G A_s$ the value of Δx would be constant. However, when taking X60 as an example, the shear force needs to be far larger than $G A_s = 1.666\text{x}10^6\text{x}0.01\text{x}0.01 = 166.6\,\text{N}$ for this to happen. $G = \frac{E}{2(1+\nu)}$ and $E = 5\,\text{MPa}$ for the X60 Filament and A_s =10 by 10 millimeters as an example of the expected area.

Meaning that this approximation only holds for values $F_s \ll G A_s$.

Capacitance

Now most factors have been taken into account and an expression for the capacitance can be determined. To find the most suitable approximation multiple criteria have to be met. First it has to take into account two parallel plates with finite length and width which also have a finite thickness.

Most approximations consist of two parallel plates of infinite length or one finite length plate parallel to an infinite ground plate as seen in Kalaiarasi et al.[12].

Kalaiarasi does mention Palmer's model [13] which determines the capacitance for two finite parallel plates. However, Kalaiarasi does not take the thickness of the plates into account. A report by Leus et al. [14] showed a combination of Palmer's model and Yang's model [14]. Palmer showed a great approximation for fringing fields and capacitance of two parallel plates. Yang empirically determined how the thickness of the plates affects the capacitance and defined another approximation for the capacitance of finite parallel plates.

Combining the two models resulted in a more precise model for two finite parallel plates of finite thickness as shown in equation 3.17 where T is the thickness of the plates.

$$C = \epsilon_0 \epsilon_r \frac{W_N L_N}{d'_N} \Bigg[\underbrace{1 + \frac{d'_N}{\pi W_N} + \frac{d'_N}{\pi W_N} ln\left(\frac{2\pi W_N}{d'_N}\right)}_{\text{Palmer}} + \underbrace{\frac{d'_N}{\pi W_N} ln\left(1 + \frac{2T}{d'_N} + 2\sqrt{\frac{T}{d'_N} + \frac{T^2}{(d'_N)^2}}\right)}_{\text{Yang/2}} \Bigg] \quad (3.17)$$

ϵ_0 is the permittivity of vacuum and ϵ_r is the relative permittivity of the material between the conductive plates.

3.1.2 Dome structure

The model for the dome structure is more complex than the three layered structure. Multiple descriptions have to be determined including the length of electric field lines between the dome and the shell. To simplify the model, the capacitive behaviour of a half cylinder with a hollow cylindrical shell is determined first. An example of this type of sensor can be seen in Figure 3.4.

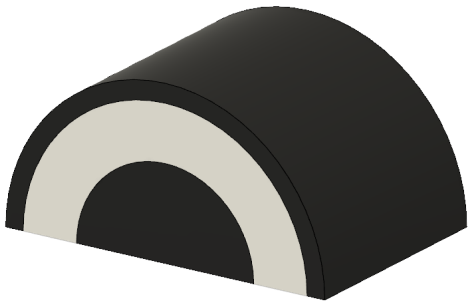

Figure 3.4: Example of a cylindrical type shear force sensor

Eccentric Cylinders

In this particular situation, there are two cylinders of radius r_1 and r_3 with centers M_1 and M_3. Both cylinders will be consisting of ETPU and the space between will be filled with the flexible filament X60. The outer cylinder will be experiencing a shear force, causing it to move along the direction of the shear force. The movement will cause the center M_3 to shift a certain distance Δx. This shift will most likely have an effect on the capacitance of the cylinder. This is shown in Figure 3.5.

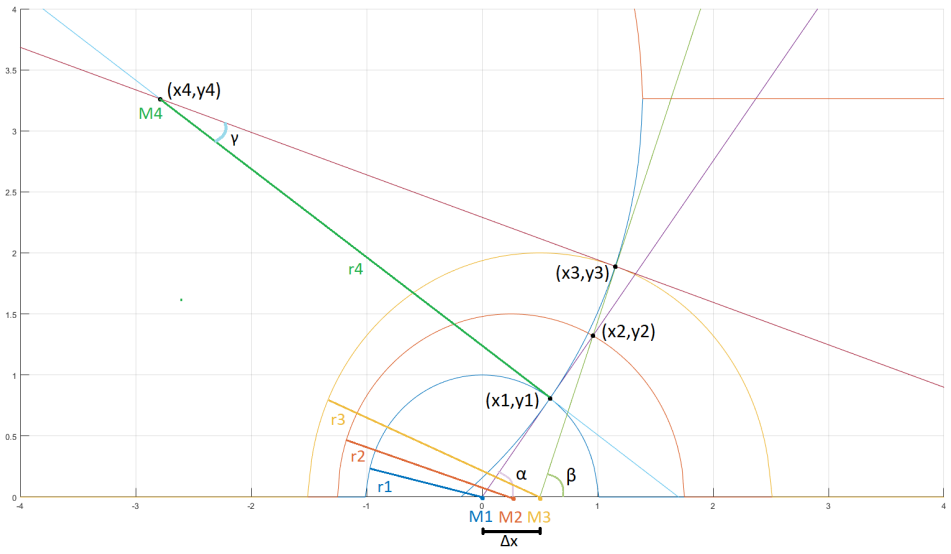

Figure 3.5: Eccentric circles with their tangents. The tangent's crossing point is the center M_4 for another circle. The radius r_4 of this circle is the distance between its center and the cylinder along the tangent of the cylinder.

Movement

To determine the capacitance change corresponding to the force applied, the movement caused by the force has to be determined first. To determine the movement, the same principles are used as mentioned in 3.1.1. The way it is implemented is shown in Figure 3.6. The parts of the X60 between the cylinders that will experience the most force are drawn as bars. To determine the horizontal movement, the space that will experience the most shear force is divided into a certain amount of small bars A_{bar} of width W_{bar} and height ΔH_{bar}. It is known that the movement caused by the shear force will be very small compared to the size of the cylinders, therefore it is assumed that the width W_{bar} of all the small bars is the same and same is assumed for the height ΔH_{bar}. Applying the principles mentioned in 3.1.1 will result in the equations shown in equation 3.18.

$$\Delta x = \frac{W_{\text{bar}} F s}{A_{\text{bar}} \Delta H_{\text{bar}} L E} \tag{3.18}$$

E is the Youngs modulus of the X60 filament and L the length of the cylinder.

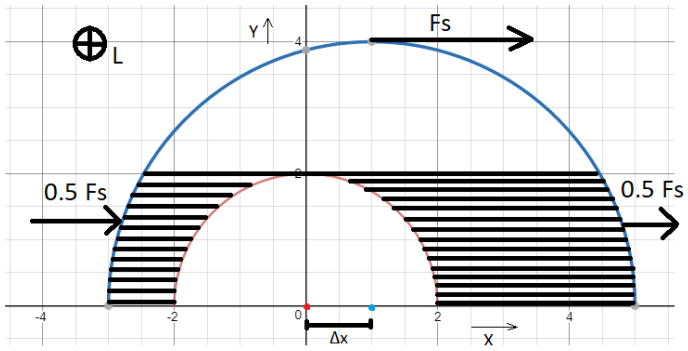

Figure 3.6: The space between the outer cylindrical shell and the inner cylindrical core filled with small bars that experience the shear force.

Field lines

A conducting cylinder inside a moving grounded cylindrical shell causes a certain capacitance to occur and it causes the field lines to curve as shown in Figure 3.7. To determine this capacitance, the angle α will be varied and for every angle the length of the field line will be determined. To determine the length of the field line, an extra half cylinder with center M_2 and radius r_2 is added which is used to determine the points on the outer cylinder where the field line is perpendicular as shown in 3.5and the shortest length. The new half cylinder in the middle of the inner and outer cylinder. The location of the center M_2 and the length of radius r_2 are shown in equations 3.19 and 3.20 and correspond with Figure 3.5.

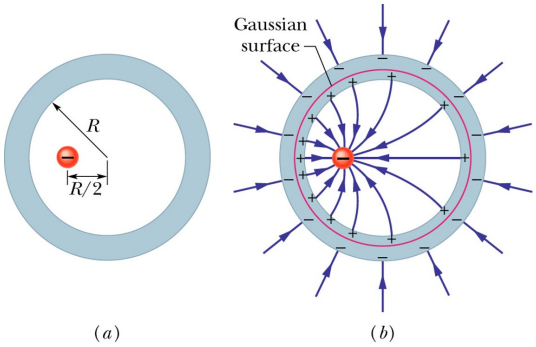

Figure 3.7: The field lines between a single charge and an eccentric cylindrical Gaussian surface.

$$M_2(x, y) = M_1(x + \frac{1}{2}\Delta x, y) \tag{3.19}$$

$$r_2 = \frac{r_2 - r_1}{2} + r_1 \tag{3.20}$$

First the points (x_1, y_1) and (x_2, y_2) on the inner cylinder and outer cylinder will be determined. These points are the intersections between the inner and middle cylinder with the line $y_\alpha = s_1 x$ where the slope $s_1 = \frac{y_1}{x_1}$.

$$x_1 = r_1 \cos(\alpha) \tag{3.21}$$

$$y_1 = r_1 \sin(\alpha) \tag{3.22}$$

$$s_1 = \tan(\alpha) \tag{3.23}$$

$$y_2 = \tan(\alpha) x_2 \tag{3.24}$$

$$y_2 = \sqrt{r_2^2 - (x_2 - \frac{1}{2}\Delta x)^2} \tag{3.25}$$

$$\tan(\alpha) x_2 = \sqrt{r_2^2 - (x_2 - \frac{1}{2}\Delta x)^2} \tag{3.26}$$

$$\tan^2(\alpha) x_2^2 = r_2^2 - (x_2 - \frac{1}{2}\Delta x)^2 \tag{3.27}$$

$$\tan^2(\alpha) x_2^2 + x_2^2 - \Delta x \; x_2 + \frac{1}{4}\Delta x^2 - r_2^2 = 0 \tag{3.28}$$

$$(\tan^2(\alpha) + 1) x_2^2 - \Delta x \; x_2 + \frac{1}{4}\Delta x^2 - r_2^2 = 0 \tag{3.29}$$

$$x_2 = \frac{\Delta x \pm \sqrt{\Delta x^2 - 4(\tan^2(\alpha) + 1)(\frac{1}{4}\Delta x^2 - r_2^2)}}{2(\tan^2(\alpha) + 1)} \tag{3.30}$$

$$y_2 = \tan(\alpha) x_2 \tag{3.31}$$

Now it is possible to determine the point on the outer cylinder where the field line that starts at point (x_1, y_1) ends. It is known that the field lines are perpendicular to the cylinders, therefore the point (x_3, y_3) on the outer cylinder, shown in Figure 3.5, will be the endpoint of the field line corresponding to the angle α and will have the shortest distance to (x_1, y_1). To find point (x_3, y_3), a new line y_β with slope s_2 and angle β has to be determined that intersects point (x_2, y_2) and is perpendicular to the outer cylinder. This means that the line has to intersect at the centre of the outer cylinder.

$$s_2 = \frac{y_2}{x_2 - \Delta x} \tag{3.32}$$

$$\beta = \arctan(s_2) \tag{3.33}$$

$$y_3 = s_2 x_3 \tag{3.34}$$

$$y_3 = \sqrt{r^3 - (x - \Delta x)^2} \tag{3.35}$$

$$s_2 x_3 = \sqrt{r^3 - (x - \Delta x)^2} \tag{3.36}$$

$$x_3 = \Delta x \pm \sqrt{\Delta x^2 - (\Delta x^2 - \frac{r_3^2}{s_2^2 + 1})} \tag{3.37}$$

$$y_3 = s_2 x_3 \tag{3.38}$$

To determine the actual length of the field line, a new circle has to be determined with center M_4 and radius r_4. The radius r_4 is the same length as the distance between the center M_4 and the points (x_1, y_1) and (x_3, y_3). To determine M_4 the tangent lines T_1 and T_2 of the inner and outer cylinder have to be determined on the points (x_1, y_1) and (x_3, y_3). The intersection of these tangents is the position of M_4. The tangent T_1 of the inner cylinder on point (x_1, y_1) can be determined using s_1. It is known that the slope of the tangent T_1 is the negative inverse of the slope s_1.

$$T_1 = -\frac{1}{s_1}(x - c_1) \tag{3.39}$$

The translation c_1 can be determined using (x_1, y_1).

$$y_1 = -\frac{1}{s_1}(x_1 - c_1) \tag{3.40}$$

$$c_1 = s_1 y_1 + x_1 \tag{3.41}$$

Same can be done for the tangent T_2.

$$T_2 = -\frac{1}{s_2}(x - c_2) \tag{3.42}$$

$$c_2 = s_2 y_3 + x_3 \tag{3.43}$$

The position of M_4 can now be determined.

$$T_1 = T_2 \tag{3.44}$$

$$-\frac{1}{s_1}(x - c_1) = -\frac{1}{s_2}(x - c_2) \tag{3.45}$$

$$x_4 = \frac{c_1 s_2 + c_2 s_1}{s_2 - s_1} \tag{3.46}$$

$$y_4 = -\frac{1}{s_1}(x_4 - c_1) \tag{3.47}$$

The radius r_4 can then be determined

$$r_4 = \sqrt{(x_1 - x_4)^2 + (y_1 - y_4)^2} \tag{3.48}$$

To determine the field line length, the angle γ between the tangent lines has to be determined.

$$\gamma = |\arctan(\frac{1}{s_1}) - \arctan(\frac{1}{s_2})| \tag{3.49}$$

The length of the field line is $d_{fl} = \gamma r_4$.

The graphs of the cylinders, $y_\alpha, y_\beta, T_1, T_2$ and the circle with center M_4 and radius r_4 can be seen in Figure 3.5. An example of the calculation of the field line per angle is shown in Figure 3.8

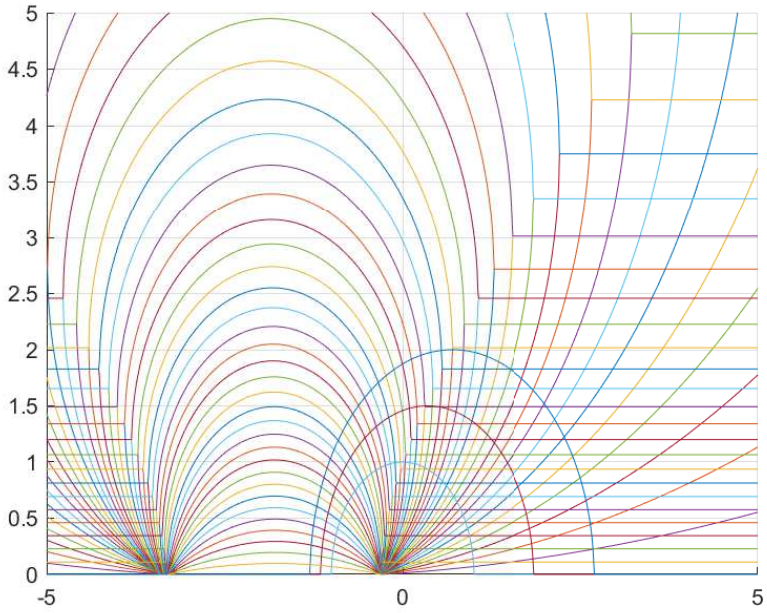

Figure 3.8: For 45 different values for α between 0 and π, the length of the field line is determined. For every angle, the field line circle corresponding to that angle is shown.

Capacitance

Once the length of the field line is determined, it is possible to apply a cylindrical Gaussian surface of radius $r1 + d_{fieldline}$ and length L. Using the Gaussian surface it is possible to determine the capacitance of two eccentric cylinders by determining the capacitance for every angle. The found capacitance will then be divided by the amount of angles. The total capacitance will then be the sum of all capacitances corresponding to every angle. An illustration of the Gaussian surfaces is shown in Figure 3.9.

$$C(\alpha) = \frac{\epsilon_0 \epsilon_r L}{\alpha \ \ln \frac{r_b(\alpha)}{r_a}} \tag{3.50}$$

The equation for a concentric conducting cylinder in a shell was used. $r_b(\alpha) = r_1 + d_{fl}(\alpha)$ is the the radius of the Gaussian surface, $r_a = r_1$ is the radius of the inner cylinder.

$$dC = C(\alpha)d\alpha = \frac{1}{2}\frac{\epsilon_0 \epsilon_r L}{m \ \ln\left\{1 + \frac{d_{fl}(\alpha)}{r_1}\right\}}d\alpha \tag{3.51}$$

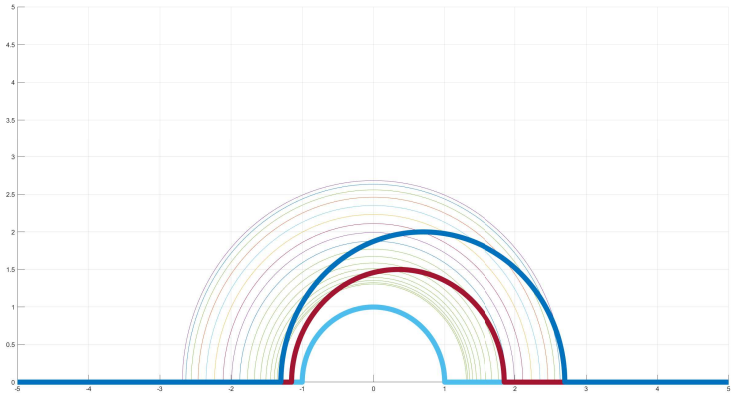

Figure 3.9: The eccentric inner, middle and outer cylinder shown as the thicker lines. Gaussian surface for every angle, shown as a thinner line. Twenty angles were approached in this graph.

$$C = \sum_{n=0}^{m} C(\alpha_{\mathrm{N}}) d\alpha \tag{3.52}$$

$$\alpha_{\mathrm{N}} = \frac{n}{m}\pi \tag{3.53}$$

m is the amount of angles considered for determining the length of the field line. The capacitance is multiplied by $\frac{1}{2}$, because the equation holds for a whole cylinder and we're only interested in one half of it. Doing so will neglect the fringing fields. However, this may be allowed since ΔC is of most interest and in the difference between $C(\Delta x)$ and $C(0)$ these fringe fields will change marginally and therefore drop.

To make the cylindrical sensor 2-DOF, the inner cylinder will be divided into two halves. To determine the capacitance of the right half with the outer shell, the capacitances for the angles from 0 to $\frac{1}{2}\pi$ will be summed and the capacitance of the left half will be the sum of the capacitances for the angles $\frac{1}{2}\pi$ to π.

3.2 Conclusions

This chapter showed the final designs chosen for the purpose of this research and the models associated with them. Multiple factors associated with the movement of the sensors components and the effects on the capacitance have been determined. The effects of shear force and normal force on the three layer sensor have been explained and approached to design an accurate approximation.

Same has been done for the effects of shear force for the cylindrical sensor. It is now possible to design a model showing the behaviour of the capacitive sensor and predict the effects of shear force on the sensor and its capacitance. Using the model it was determined that the three layer sensor is expected to be in 1 pF range and the cylindrical sensor in the 10 pF range for shear forces ranging from zero to ten Newton. The validity of these results will be checked using measurements which are further explained in Chapter 5.

Chapter 4

Fabrication

To produce the sensors described in Section 2.6, 3D-printing will be implemented as mentioned in Chapter 1. The 3D-printer used for this research will be the Flashforge Creater Pro [16]. This 3D-printer uses a printing method called Fusion Deposition Modelling (FDM) [17]. The Flashforge contains a dual extrusion system, meaning it has two nozzles available for printing at one time. This opens the possibility of printing complicated designs consisting of two materials. Additionally the printer has been customized with a dedicated extruder for flexible materials called Flexion Extruder [18].

4.1 Materials

The materials used in this research consist of a carbon doped thermoplastic poyurethane (ETPU) which is a flexible material with carbon black filler which is bound in the base polymer. The version of ETPU used is PI-ETPU 85-700+ Carbon Black which is not commercially available at this moment. This version of ETPU is sold to the University of Twente in exchange for information regarding the material. The idea is to eventually release the PI-ETPU 85-700+ for commercial use. The difference between PI-ETPU 85-700+ and the commercially available PI-ETPU 95-250 [19] is the 85 shore A hardness compared to 95 shore A and a 700% stretch compared to 250%. The dielectric materials available are NinjaFlex [20] and X60 [21] both flexible materials.

Knowing that a shear force will be applied to the surface off the sensor causing a movement which depends on the flexibility of the material between the conductive surfaces. It would be most beneficial to select the material which is most flexible. This would mean that the X60 filament would be the best choice for it has a lower Young's modulus of 5MPa [21] compared to Ninja Flex's 12MPa [20] and it has a lower hardness of Shore 60A compared to Shore 85A.

4.2 Samples

In order to find the limits of the 3D-printers printing capability, samples will be fabricated to determine the minimal spacing the printer is able to produce.

Using the calculations mentioned in 3.1, it has been determined that having the space between the two conductive plates and cylinders completely filled with the flexible material will not cause enough movement of the upper layers. This results in a minimal change of Δx and thus a minimal capacitance change.

Measurements will be executed using a HP 4284A LCR meter [22]. This LCR has a basic accuracy of 0.05% and a measurement range of 0.01 fF to 9.99 F. To prevent noise from overly affecting the measurement results, it is preferred to have a base capacitance over 1 pF and a ratio of change ($\frac{\Delta C}{C}$) of over 0.1%.

An option to increase the ratio of change and base capacitance, is to decrease the area over which the shear force is exerted. This will increase the horizontal and vertical movement causing a greater change in capacitance. This can be accomplished by using the example mentioned in 1.3.2 where the flexible material between the plates is divided into separate parts of smaller sizes, causing the three plate structure to become more flexible structure.

This means that the sensor will have air pockets, and they will have to be printed with the air pockets vertically as shown in Figure 4.4. Due to printing limitations the dome will become a cylinder since it cannot be printed in free air, the design will then look like Figure 4.1.

Figure 4.1: Cylindrical sensor with smaller flexible bars.

Using the model it was determined that the thinner the flexible material is between the ETPU, the more change will occur in the horizontal and vertical movement, causing a bigger change in capacitance for the same amount of force. To determine the smallest size, samples will be printed to determine the smallest distance between the conductive material and the smallest parts of flexible material the printer can extrude.

4.2.1 Printing

The 3D-printer is fitted with nozzles with a diameter of 0.4 mm and 0.6 mm. The ETPU will be printed using the 0.6 mm nozzle and the X60 using the 0.4 mm. To determine the minimum distance possible between the conductive material, multiple structures of two lines of ETPU are printed with different spacing between them and different sizes of flexible material as shown in Figure 4.2

and 4.3. To design the 3D model, the CAD program Fusion 360 by Autodesk [23] is used.

The 3D-printers path and other parameters such as extrusion speed and temperature are determined by a so-called slicer software. This is a piece of software that converts a CAD-design, to a format the 3D-printer can read and follow. The software used for this research is called Simplify3D [24]. The settings used for the X60 and ETPU by the slicer are mentioned in Table 4.1.

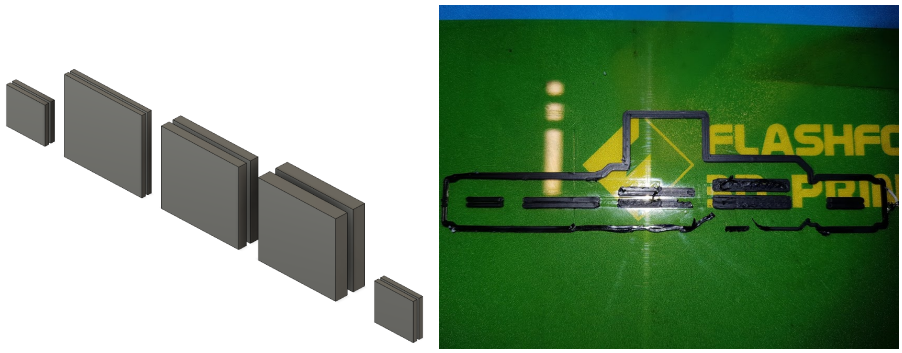

(a) 3D-model (b) Printing results

Figure 4.2: Test to determine the minimal distance between the ETPU layers ranging from 0.5 mm to 1.5 mm.

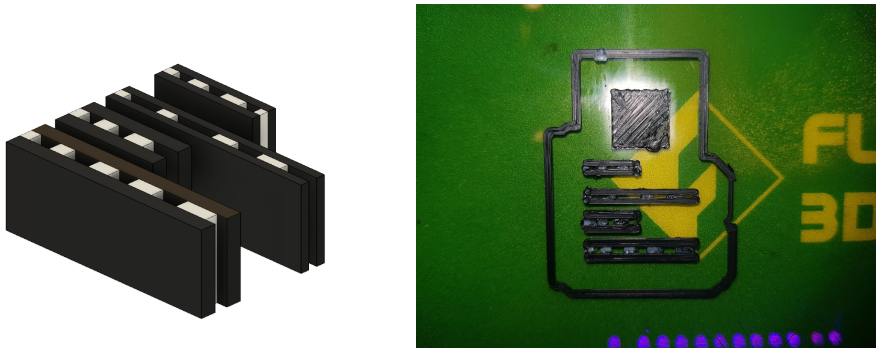

(a) 3D-model (b) Printing results

Figure 4.3: Test to determine the minimal width of the X60 ranging from 0.5 mm to 3 mm for ETPU distances of 1 mm and 1.2 mm.

As can be seen from Figure 4.2b, the smallest possible distance between the ETPU was determined to be 1 mm with a minimal width of X60 of 0.5 mm as can be seen in Figure 4.3b. It is believed that these values cannot be decreased because of a so called Die Swell effect, also known as extrudate swell. Die-swell happens when a polymer stream is compressed by entrance into a nozzle

for example and is followed by a partial recovery or "swell" back to its former shape and volume [25]. It was noticed that it is possible to decrease the amount of adhesion between the X60 and the ETPU by printing the X60 slightly smaller than the distance between the ETPU as shown in Figure 4.4.

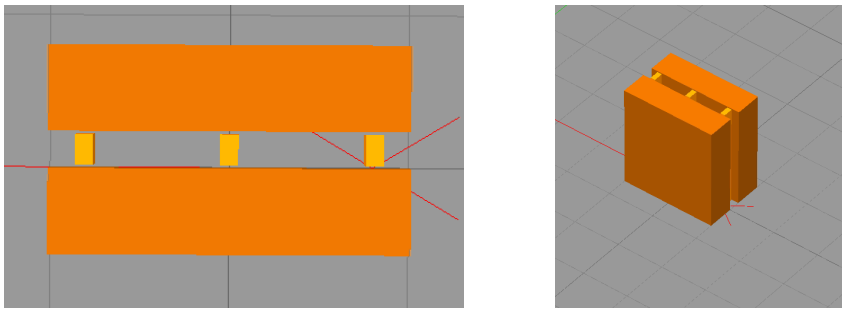

(a) Top down view of the slicer model. (b) 3D view of the slicer model.

Figure 4.4: Final slicer model used to print the three layered sensor

The extrusion multiplier plays a certain role in the amount of filament that is extruded. Increasing the multiplier will increase the flow rate and in turn the amount of filament extruded. In the case of more flexible filaments, which are more difficult to extrude, the extrusion multiplier is most often higher than 1. The extrusion multiplier is empirically determined by executing multiple prints and determining if the size of the prints corresponds with what is expected. If the print contains hollow spots and was too thin, the extrusion multiplier was not high enough. If it was too thick, the extrusion multiplier was too high. For X60 it was determined that the extrusion multiplier should be 1.5.

The printing speed is fairly low, because the sensors are printed thin and high, having little surface contact with the printing bed which at high speeds could cause the printed sensor to let go from the bed during printing. The primary layer height for the X60 is higher to prevent the extruded material from being pushed down and smearing out causing a larger adhesion area to the ETPU.

When using two extrusion nozzles side by side, it happens that one nozzle runs through printed material from the other nozzle causing the first nozzle to have other filament on it. This could mix with the contents of the first nozzle and cause dripping. Prime pillars are used to prime the nozzle for printing in case leakage occurs causing the printer to print air until the filament catches up again. Another use is to prevent the dripping in the printed sensor. It is used to make sure the printed material from the nozzle is not contaminated with another filament.

Table 4.1: Settings used in Slicing software

	Nozzle Diameter	Extrusion Multiplier	Primary Layer Height	Prime Pillar	Temperature	Speed
X60	0.4 mm	1.5	0.4 mm	Yes	210	200 mm/s
ETPU	0.6	1.25	0.2 mm	Yes	220	1000 mm/s

4.3 Conclusions

The printing limits of the 3D-printer have been approached and the slicer settings have been set accordingly. It was determined that the minimal distance between two ETPU layers has to be at least 1 mm, taking into account the dripping and smearing of the filament during printing. The size of the X60 has been determined to be 0.5 mm by 1 mm to have the desired amount of adhesion to the ETPU.

Chapter 5

Method

To determine the most accurate results whene executing the measurements, it is important to first determine the way the capacitance will be measured and the force will be applied. This chapter will explain the measurement setup and what tools and equipment was used to measure the most accurate result.

5.1 Sensor printing

To have the most accurate print corresponding to the model, some alterations to the printed product have been made. It was noticed that the first printed layer turned out wider than anticipated as shown in Figure 5.1. This caused short-circuits but only in the first layer. To combat this, the height of the print was increased by 1 mm and the first layer was then cut off with a scalpel resulting in a practically short-circuit free structure.

Copper wires connected to headers were melted into the print by heating a soldering iron to the melting temperature of the ETPU and melting the ETPU where the wires were supposed to be connected. For the three layered structure four wires were melted into the print, on each side of the print as shown in

Figure 5.1: First layer of the printed three layered structure

Figure 5.2. For the cylindrical structure six wires will be melted into the sensor, two wires for each half of the inner cylinder and two on the outer shell as shown in Figure 5.3. Four wires are used to make a four point measurement possible. A schematic overview of the measurement setup is shown in Figure 5.4 for both the three layered design and the cylindrical design.

For the Cylindrical sensor, an extra bar of ETPU was added to the top shell to create a better surface for the force to be applied on. This extra bar will fit into the printed support designed for it mentioned in Section 5.2 and make the outer shell more pinned to the designed support. The bottom of the inner cylinder is elongated by 3 mm to be able to pin the inner cylinder down separately from the outer shell. Both the extra as the elongation can be seen in the final print shown in Figure 5.3. The final dimensions of the three layered design are shown in Table 5.1, for the cylinder design it is shown in Table 5.2.

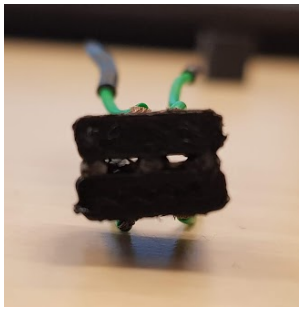

(a) Front view

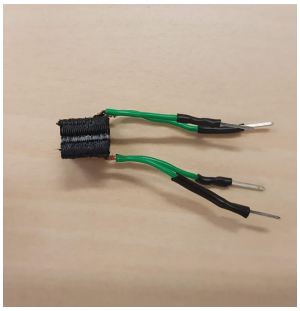

(b) Side view

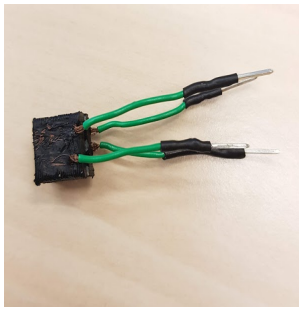

(c) Top view

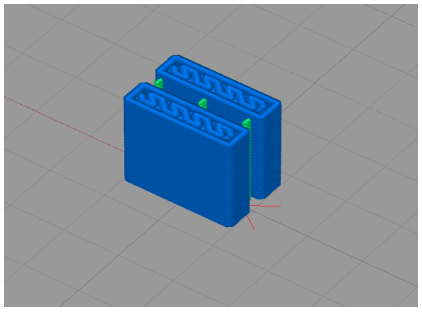

(d) 3D-view of the 3D-printing simulation for the three layer structure

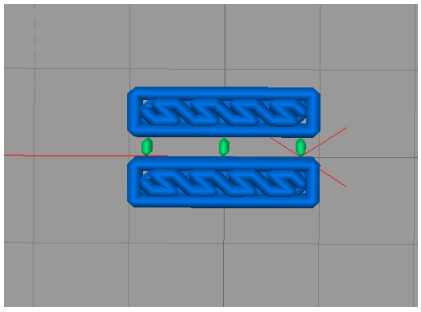

(e) Top view of the 3D-printing simulation for the three layer structure

Figure 5.2: Front, side and top view of the final three layered structure print and the 3D-printing simulation.

5.2 Printed supports

To apply the desired amount of shear force to the sensor and keep the sensors base static, supporting aids are designed using Fusion 360 and Simplify3D to

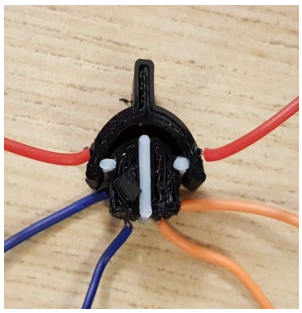

(a) Front view

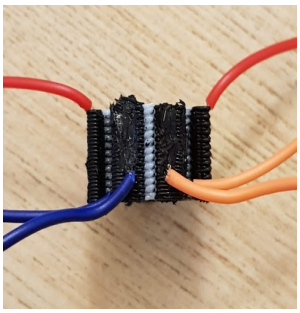

(b) Bottom view

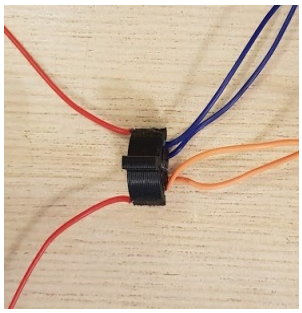

(c) Top view

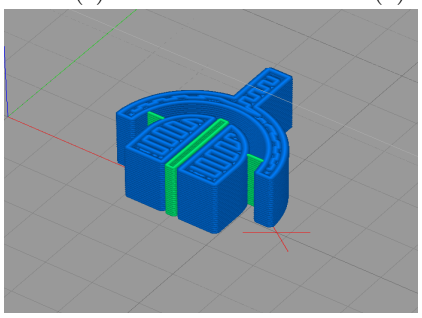

(d) 3D-view of the 3D-printing simulation for the cylindrical structure

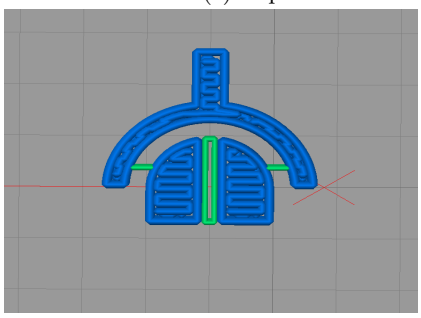

(e) Top view of the 3D-printing simulation for the cylindrical structure

Figure 5.3: Front, bottom and top view of the final cylindrical structure print and the wires used for measurements

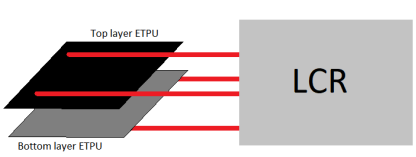

(a) Three layered structure

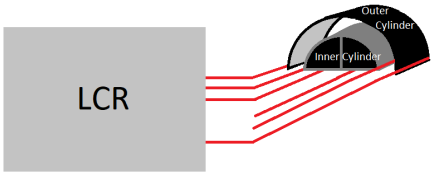

(b) Cylindrical structure

Figure 5.4: Schematic overviews of the 4-points measurement setup for the three layered and cylindrical structures

help with the measurement. These aids are printed using basic ABS plastic filament. The first needed support was an item to hold the lower layer of ETPU in place when a shear force is applied to the top layer. This is done by designing a larger piece of ABS with a hole in it of the same size and the sensor, so 10 mm by 10 mm. The designed model and print can be found in Figure A.1 in A of the Appendix.

To apply the right amount of shear force on the top surface of the sensor,

	Thickness	Length	Width
ETPU	3 mm	10 mm	10 mm
X60	1 mm	10 mm	0.5 mm

Table 5.1: Table containing the final dimensions of the three layered shear force sensor.

	Radius	Thickness	Length	Width	Height
Inner Cylinder	10 mm	-	10 mm	-	-
Outer Cylinder	12 mm	2 mm	10 mm	-	-
X60 Inner	-	-	10 mm	1 mm	10 mm
X60 Outer	-	-	10 mm	1 mm	0.5 mm

Table 5.2: Table containing the final dimensions of the cylindrical shear force sensor.

another support was designed which would translate horizontally applied normal force to shear force on the top of the sensor. This was done by designing a tool similar to the holder shown in Figure A.1, but smaller and thicker. The thickness of the upper ETPU layer is not large enough to properly apply force using the linear actuator mentioned in section 5.3.1. Using this tool, it would be possible to apply the force using the whole surface of the actuator. The tool needs to be smaller to keep any unwanted moment to a minimum and thicker to keep it as stable as possible when a force is applied. The force will be applied at the same height as the top layer of ETPU as shown Figure A.4 to prevent any more unwanted moment. A support for the cylindrical sensor was designed in the same fashion as shown in Figure A.3

The depth for the top and bottom sensor holders for the three layered sensor is 3 mm respectively leaving enough space between the holders for the X60 not to be obstructed in its movements as can be seen in Figure A.4. For the cylindrical holder, the depth for the top layer is 1 mm, the bottom holder for the three layered sensor is reused for the cylindrical sensor. The force is then applied to the side of the cylindrical holder as shown in Figure A.5.

5.3 Measurement setup

5.3.1 Force and Movement

The force is applied and measured by a linear actuator (SMAC LCA25-050-15F) [26] and the displacement is measured as well. The SMAC Actuator has the ability to apply a specific force and determine the precise position. The force can be controlled from zero to maximum twelve Newton and can be looped. The force exerted was ranging from zero to twelve Newton with steps of 0.1 Newton which was held constant for 0.1 seconds. A total of twenty measurements were executed one after another with increasing and decreasing force as shown in

Figure 5.5.

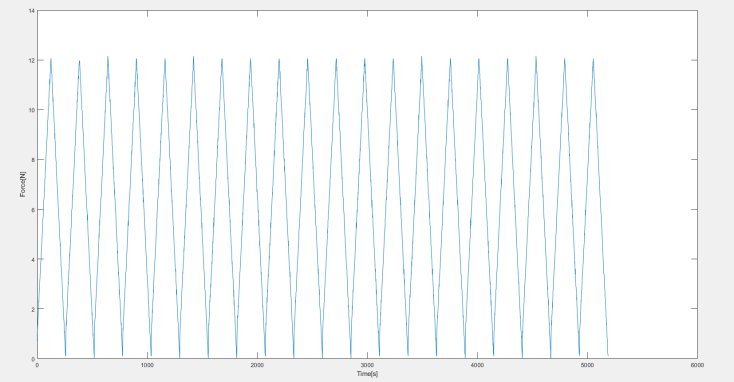

Figure 5.5: The application of force on the measurement setup.

This actuator is capable of measuring the force and the change in the position simultaneously.

5.3.2 The Setup

Figures 5.6 and 5.7 show the mounting of the sensor in the measurements setup. The force applied on the top layer will linearly increase and decrease from zero to twelve Newton and the capacitance, impedance, movement and applied force are measured using the LCR and the SMAC actuator.

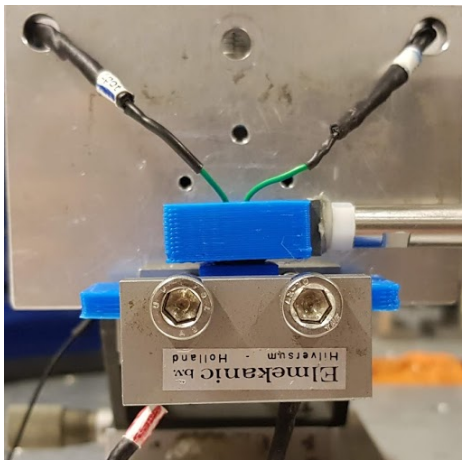

Figure 5.6: Final measurement setup where a SMAC actuator exerts a fluctuating force on the top layer holder for the three layered structure

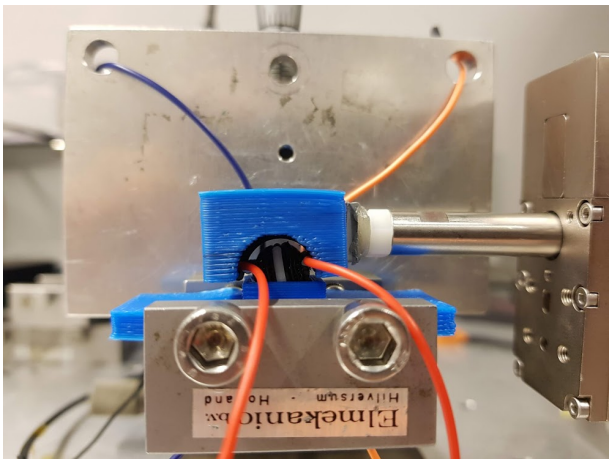

Figure 5.7: Final measurement setup where a SMAC actuator exerts a fluctuating force on the top layer holder for the cylindrical structure

5.4 Conclusions

This chapter highlighted the issues with 3D-printing and how these could be solved, e.g. cutting short-circuits off the print. The final prints and their dimensions were shown in Table 5.2 and 5.1. Certain helpful tools were designed and 3D-printed to be certain that the bottom of the sensor is immobile and the top moves due to an applied force.

Chapter 6

Results

Th experiments described in Chapter 5 are executed. The results from these experiments are shown and compared to the determined models shown in Chapter 3. The parameters necessary for the models corresponding to the printed structures are shown in Table 6.1. The parameters are measured, known constants or given by the manufacturers.

6.1 Impedance spectrography

To have the most accurate capacitance measurements, the ideal measurement frequency needs to be determined. This is done by executing impedance spectrography using the LCR. The LCR is controlled using Matlab[27] by automatically changing the measurement frequency and measuring the impedance and phase. To measure the biggest change in capacitance and have the least amount of parasitic capacitance, it is important to find the right measurement frequency. As can be seen in the impedance spectrographies shown in Figures 6.1 and 6.2, there is a certain point where the impedance of the sensor starts decreasing for a higher measurement frequency.

It was determined that this decrease also happens for the capacitance. To measure the highest change in capacitance with the best available accuracy, the measurement frequency should be at the tipping point of the impedance sepctrography. From Figure 6.1 it can be seen that the tipping point is at 1 kHz for the three layered structure. For the Cylindrical structure it can be seen from Figure 6.2 that the tipping point is at 20 kHz.

Parameter	*Value (Three layered structure)*	*Value (Cylindrical structure)*
ϵ_0	$8.854 \times 10^{-12}\,\mathrm{F\,m^{-1}}$	$8.854 \times 10^{-12}\,\mathrm{F\,m^{-1}}$
ϵ_r	1.00058986	1.00058986
E	5 MPa	5 MPa
μ	0.5	0.5
Width ETPU (W)	10 mm	-
Length ETPU (L)	10 mm	10 mm
Thickness ETPU (T)	3 mm	-
Width X60 (W_{beam})	10 mm	1 mm
Length X60 (L_{beam})	0.5 mm	10 mm
Thickness X60 (T_{beam})	1 mm	0.5 mm
Shear Force (F_s)	0-12 Newton	0-12 Newton
Normal Force(F_n)	0	-
Radius inner cylinder(r_1)	-	10 mm
Radius outer cylinder(r_2)	-	12 mm

Table 6.1: Table containing all parameters applied in the model determined in 3.1

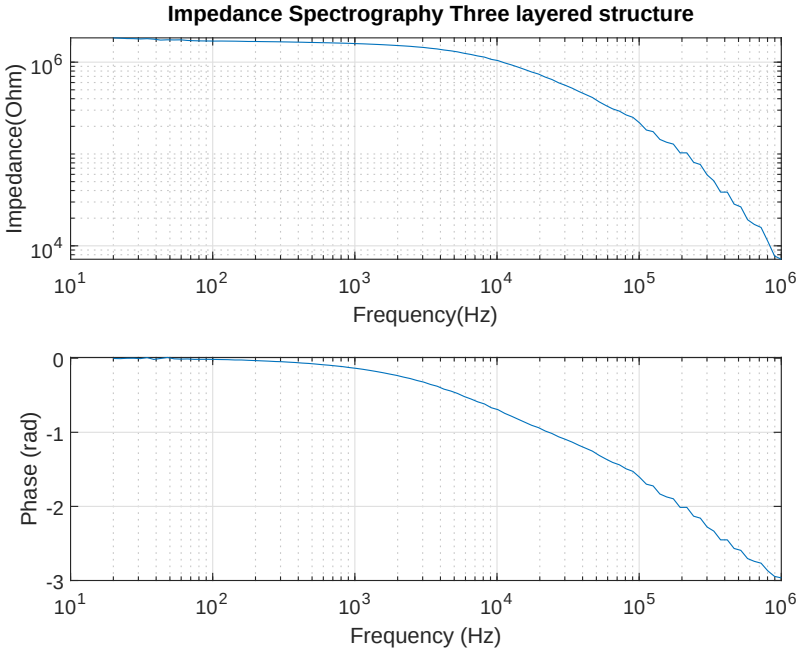

Figure 6.1: Spectrum Analysis of the Three layered structure showing the impedance and phase response to the measurement frequency.

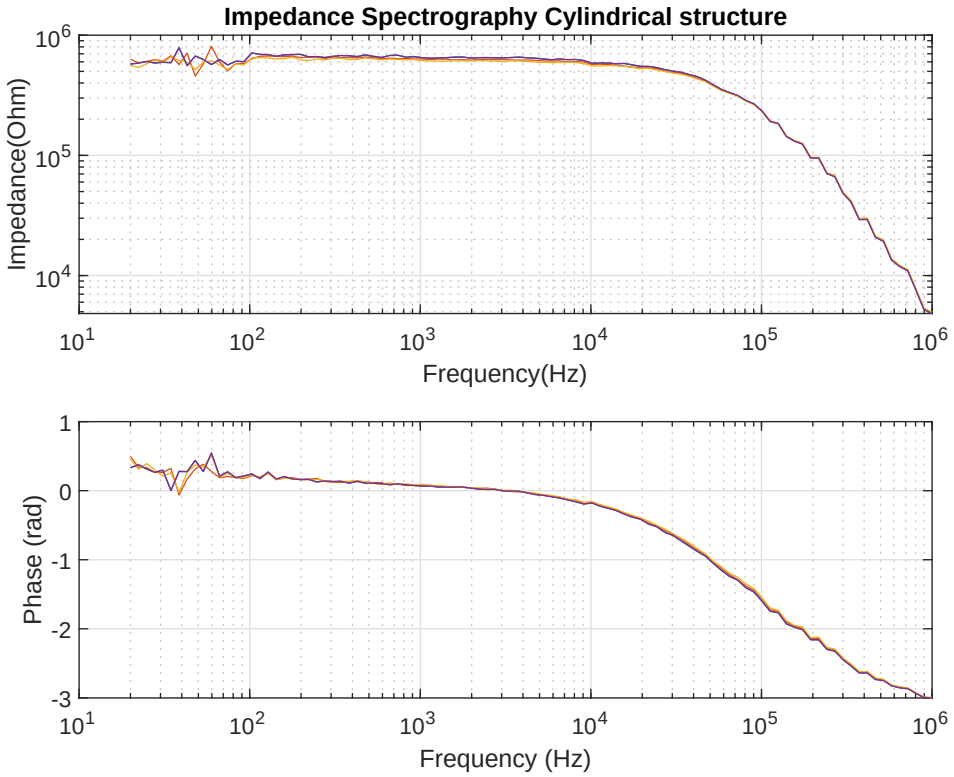

Figure 6.2: Spectrum Analysis of the Cylindrical structure showing the impedance and phase response to the measurement frequency.

6.2 Capacitance measurement

6.2.1 Displacement and Capacitance

Three layered structure

It is shown in Figure 6.3 that the model shows a decrease in capacitance before increasing. Meaning the calculated model is curved at shear force of 0 and not flat. This is most likely caused by the fact that for small forces, the horizontal displacement has a larger effect on the capacitance than the vertical displacement causing a decrease in capacitance instead of an increase. When the shear force reaches a certain value, the vertical displacement will become dominant and cause an increase in capacitance.

The resulting measurement for the three layered structure regarding the horizontal movement of the top plate and the capacitance behaviour are shown in Figure 6.3. Figure 6.4 shows the measured and modelled capacitance increase

not including the base capacitance, e.g. $\Delta C(\Delta x)$. It can be seen that for forces below two Newtons, the capacitances do not change sufficiently even though the horizontal displacement does occur. This means that the effective force measuring range is between two and twelve Newtons.

Cylindrical structure

For the cylindrical structure, the horizontal movement, the capacitance for the left and right half of the inner cylinder and the total capacitance are shown in Figures 6.5 and 6.6. Figure 6.7 shows the capacitance increase $\Delta C(\Delta x)$ of the capacitance for both sides of the inner cylinder without the base capacitance. The measurement results of the cylindrical sensor do not correspond to the determined model. Both sides of the inner cylinder show different behaviour from what was predicted, especially the side experiencing an increase in distance to the outer shell. The measured result for that side was the complete opposite of the model.

In Figure 6.6 it can be seen that the movement does not start increasing until two Newtons are applied, however there is a capacitance increase upward of one Newton. This could be a measurement error caused by the linear actuator. It is possible that the movement sensor of the actuator was at its limits and the small movement was not measured. There could have been an increase in force causing the increase in capacitance, but the actuator was not able to measure the movement.

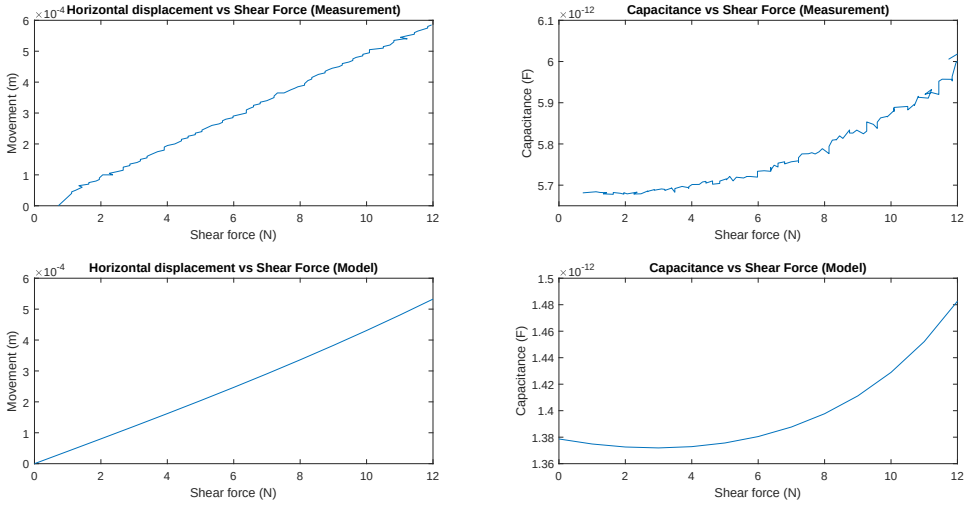

Figure 6.3: The horizontal movement and capacitance modelled and measured over increasing shear force for the three layered structure.

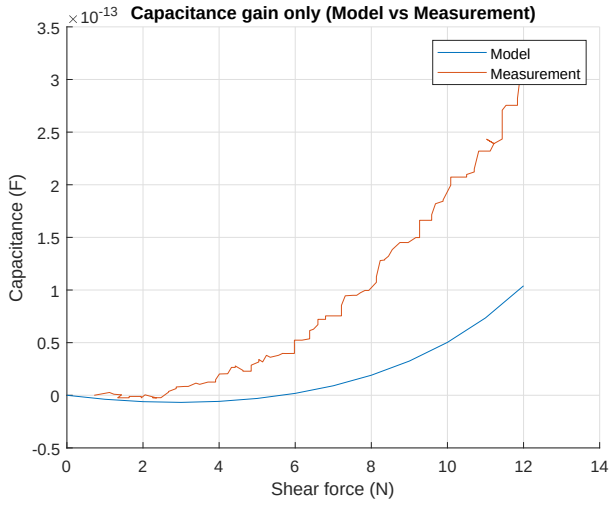

Figure 6.4: The capacitance increase $\Delta C(\Delta x)$ without the base capacitance modelled and measured over increasing shear force for the three layered structure.

6.2.2 Plastic deformation

Figure 6.8 shows the capacitance per amount of force over time. The more time passes, the less the base capacitance becomes of the three layered sensor. This is most likely caused by plastic deformation occurring in the sensor, making the sensor not return to its original state. Figure 6.9 also shows the capacitance over time for the cylindrical sensor, except in this case the capacitance increase $\Delta C(\Delta x)$ increases over time. Plastic deformation is a recurring phenomenon in research regarding 3D-printed sensors, as can be seen in reports by Wolterink et al.[6] and Schouten et al.[28].

6.3 Conclusions

The measurements showed that a change in shear force does show a change in capacitance for both sensors. The three layered sensor experiment showed results relatable to the designed model. The base capacitance was different, but the gain was close to the measured value. This could be caused by an incorrect dimension measurement of the three layered sensor.

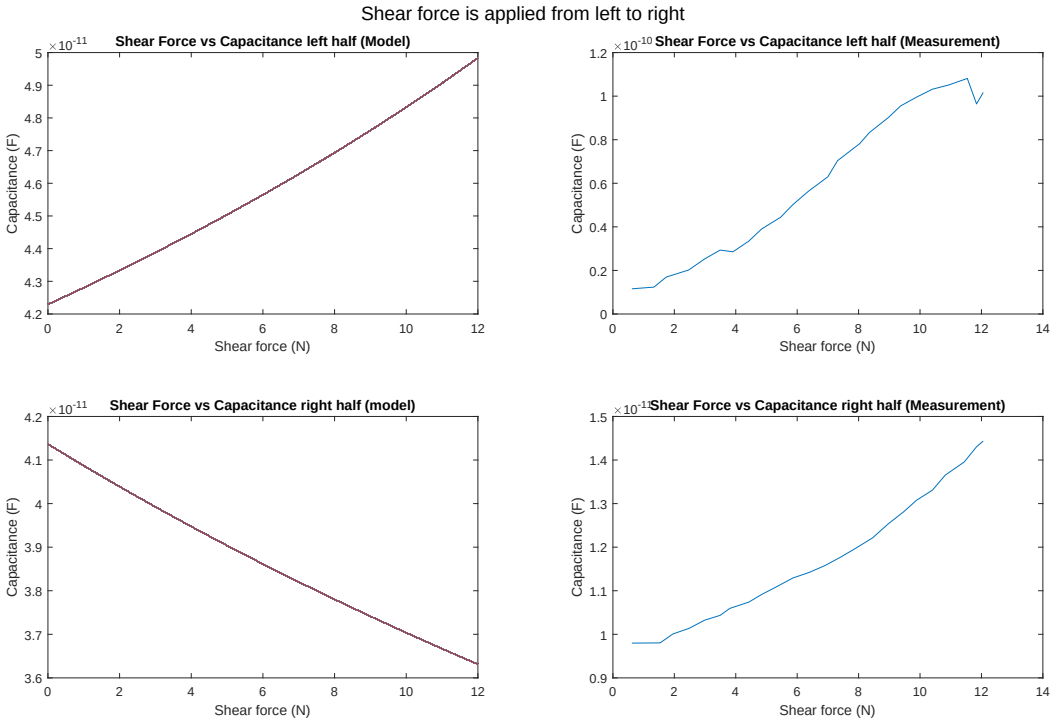

Figure 6.5: The capacitance for the left and right half of the inner cylinder modelled and measured over increasing shear force.

Measurements for the cylindrical sensor showed vastly different results compared to the model. The cylindrical sensor did show a change in capacitance for an acting force. However, it was unrelated to the model. It is likely the cylindrical sensor's movements and dimensions behaved much different from what was assumed, causing this large difference.

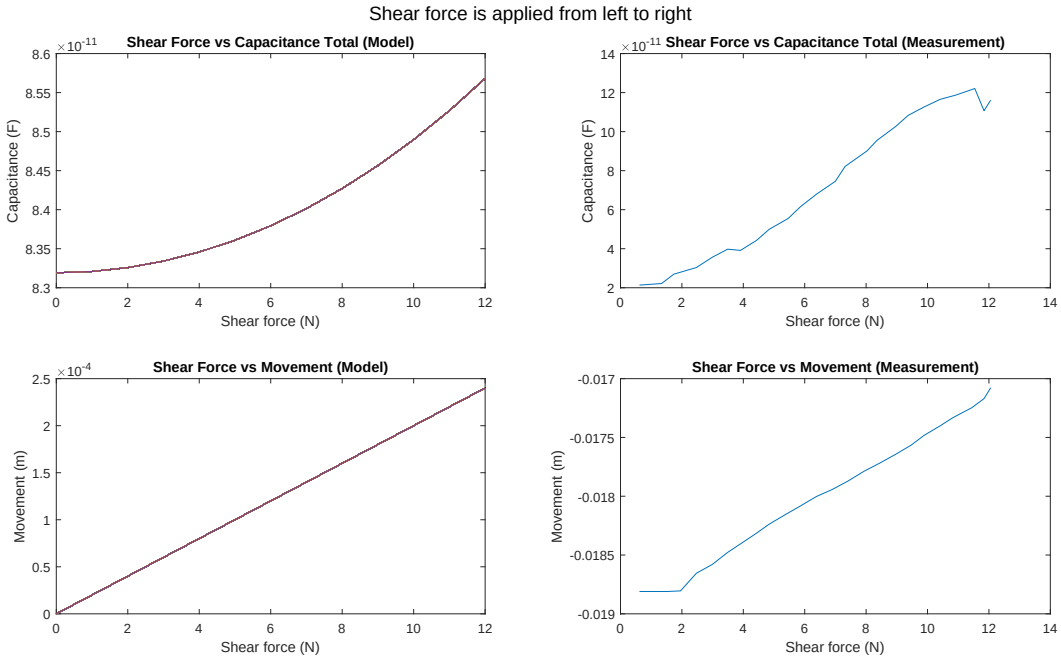

Figure 6.6: The capacitance for the left and right half of the inner cylinder modelled and measured over increasing shear force.

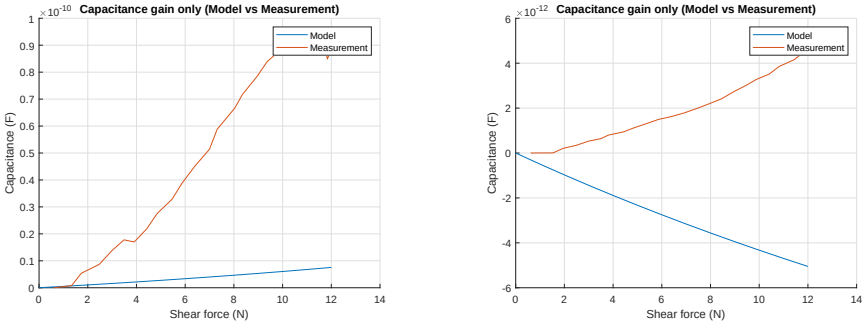

(a) For the inner cylinder side experiencing a decrease in distance to the outer shell cylinder.

(b) For the inner cylinder side experiencing an increase in distance to the outer shell cylinder.

Figure 6.7: Measured capacitance increase $\Delta C(\Delta x)$ without the base capacitance for both sides of the inner cylinder compared to the modelled capacitance increase.

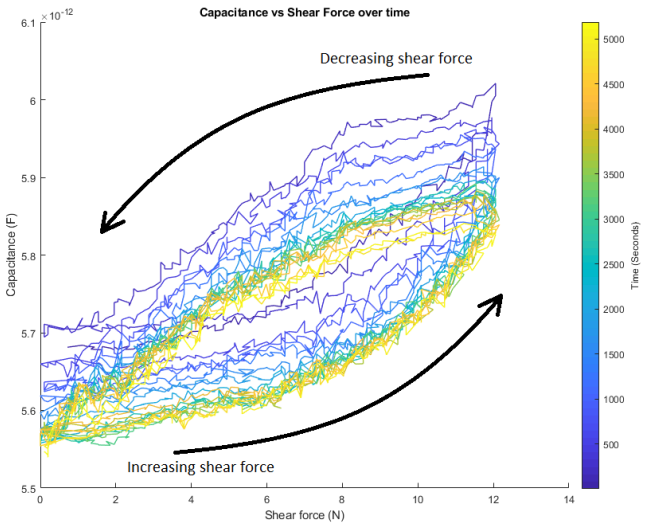

Figure 6.8: Twenty measurements of the capacitance of the Three layer structure for an applied shear force as shown in Figure 5.5 over time.

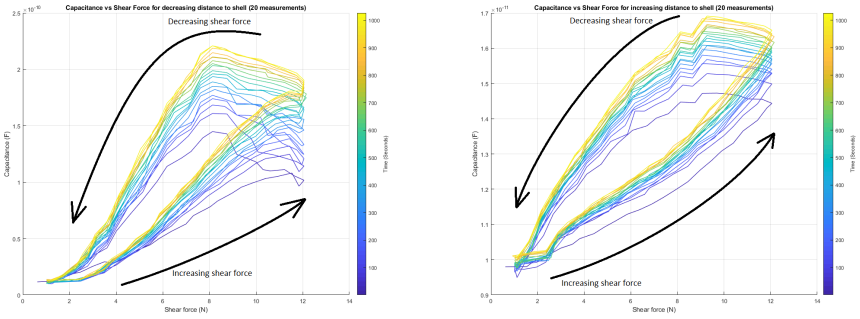

(a) For the inner cylinder side experiencing an increase in distance to the outer shell cylinder

(b) For the inner cylinder side experiencing a decrease in distance to the outer shell cylinder

Figure 6.9: Twenty measurements of the capacitance versus the shear force over time. This capacitance is measured for both sides of the inner cylinder.

Chapter 7

Discussion

7.1 Three layer structure

As can be seen from Figure 6.3, the model has roughly the same shape as the measurements as can be seen in Figure 6.4.

The shape of the graph is most likely caused by the non linear increase of capacitance that happens because of the vertical and horizontal movements of the top layer that depend on the angle α.

The increase in capacitance per Newton of the model is roughly $\frac{1}{3}$ of the measurement. This is most likely caused by the fact that it is very difficult to determine the actual dimensions of the sensor. The size of the sensor makes the distance between the ETPU layers and the amount of area that adheres between the X60 and the ETPU very difficult to determine.

During printing, the filament is extruded and then spread with the nozzle, causing the distances to be different from what is designed. These small changes have large effects on the results of the capacitance and horizontal movement. A difference of 100 µm can cause the horizontal movement and capacitance increase to be much different. As an example, when changing the value of L_{beam} from Table 6.1 to 0.4 mm, the capacitance and horizontal movement model is much more like the measurement as shown in Figures 7.1 and 7.2. However, the model does still have a non-symmetric response, meaning that it is still not as accurate as desired.

There is also a difference in base capacitance of the model and measurement of roughly 5 pF. This can be caused by the fact that multiple unshielded wires were soldered into the sensor, adding parasitic capacitance to the measurement. A remedy could be to replace the unshielded wires for shielded wires or to decrease the size of the unshielded wires to the minimum.

When a normal force is applied to the sensor, the base capacitance is expected to change as shown in Figure 7.3. This would mean that if the normal force acting on the sensor is fluctuating, the resulting measured capacitance will be unrelatable to the shear force and render the sensor useless. This means that

a stable normal force is required for the sensor to operate optimally.

The drift shown in Figure 6.8 can be caused by small movements of the bottom layer. It is possible it is not properly clamped by the holder and moves every time a force is exerted on the top layer. It is also possible the small parts of X60 experience so much force that they stretch and do not return to their original shape, causing plastic deformation. A clear relationship between the drift and time has not yet been observed.

7.2 Cylindrical structure

The capacitances measured for the cylindrical sensor do not correspond with the model. The capacitance increase of the model is a factor ten smaller than the measurements for the inner cylinder side experiencing a decrease in distance to the outer shell. The other side experienced an increase in capacitance instead of a decrease which was expected. A few reasons for this behaviour can be considered. The first is the fact that the flexibility of the sensor causes the sensor to deform in a way as shown in Figure 7.4. This deformation causes the distances between the cylinders, therefore the capacitances, to be uncorrelated to the model. For the model it was assumed that two cylinders are measured and the outer cylinders position only translates. This is in reality not the case, making the determined model inaccurate. This was a first attempt to model such a complex geometry and it might be of use if more research using this geometry is conducted in the future. It could be possible to create a sensor correlating to the model by making the conductive part of the sensor stiffer to prevent behaviour as shown in Figure 7.4.

A capacitance change was still measured as shown in Figures 6.7 and 6.5. However, a new model has to be determined to properly use these results. It was seen that the capacitance for an expected increase of distance to the shell, also increased. This too, can be explained by the fact that the sensor deforms under shear force causing unexpected behaviour.

This sensor also showed drift. Except, in this sensor's case the capacitance increase $\Delta C(\Delta x)$ increased over time. This could be caused by the fact that the sides of the cylindrical sensor are pushed together causing the X60 between the ETPU to be compressed and experience plastic deformation like the three layered sensor.

7.3 Suggestions

Printing resolution One of the main problems with the sensor is the printing resolution. To create small sensors, a high resolution 3D-printer is needed. The nozzle size and the diameter of the filaments all play a large role in the amount of filament that is extruded and how much smearing occurs. It would be possible to decrease the amount of smearing by using thinner nozzles to increase the printing resolution. However, this could come at the cost of many irregularities

due to clocking and unstable materials extrusion.

Accurate dimension Finding the most accurate dimensions plays a large role in having an accurate model. Finding an accurate way of measuring the distance between the ETPU layers and the size of the X60 beams will hugely affect the model and help with making more accurate predictions.

Making the conductive part stiffer It would also be interesting to make the conductive parts of the sensors stiffer by maybe using other conductive filaments or by increasing amount of layers of the flexible filament to see if this results in an increase of capacitance per newton. The ETPU is flexible and can be bent easily, which can affect the capacitance measured. Making it stiffer could have a more linear effect on the capacitance compared to the more flexible prints. Flexibility adds another factor that needs to be taken into account, which can be negated by making the conductive parts stiffer.

New model A main point of interest would be to determine how exactly the flexible ETPU in the cylindrical structures case deforms and determine its effect on the capacitance of the whole structure. A camera could be used to observe the movements of the cylindrical structure during experiments.

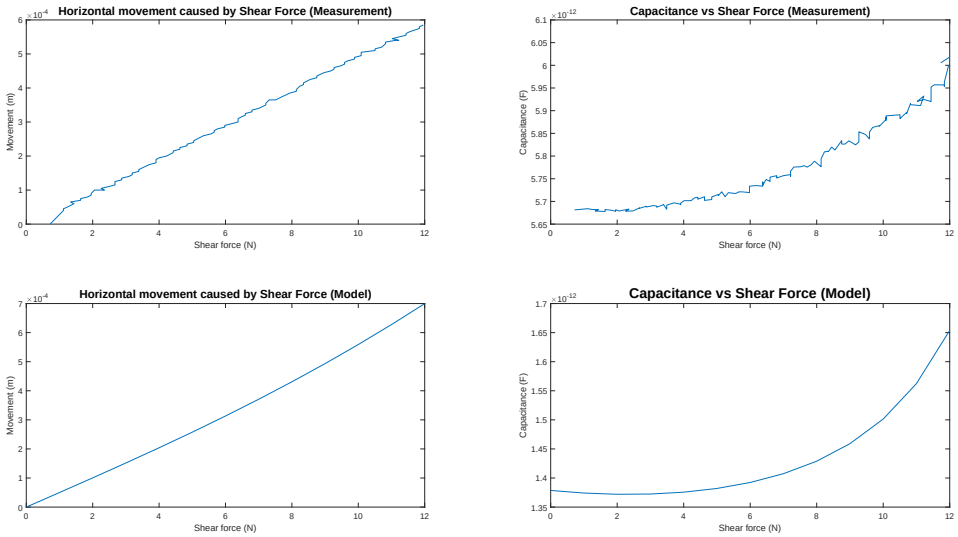

Figure 7.1: The horizontal movement and capacitance modeled and measured over increasing shear force for a smaller L_{beam}.

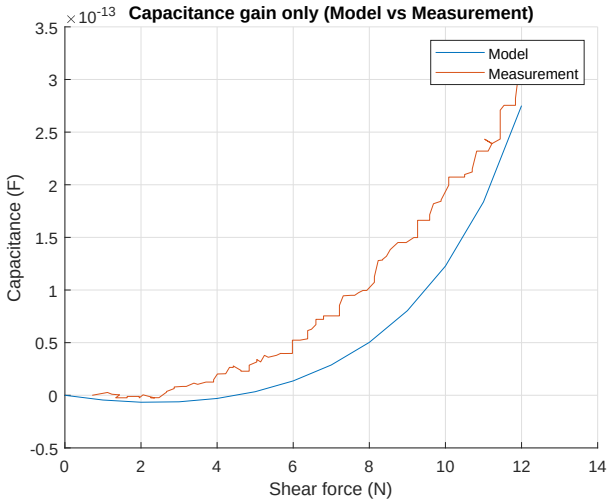

Figure 7.2: The capacitance increase $\Delta C(\Delta x)$ without base capacitance modeled and measured over increasing shear force for a smaller L_{beam}.

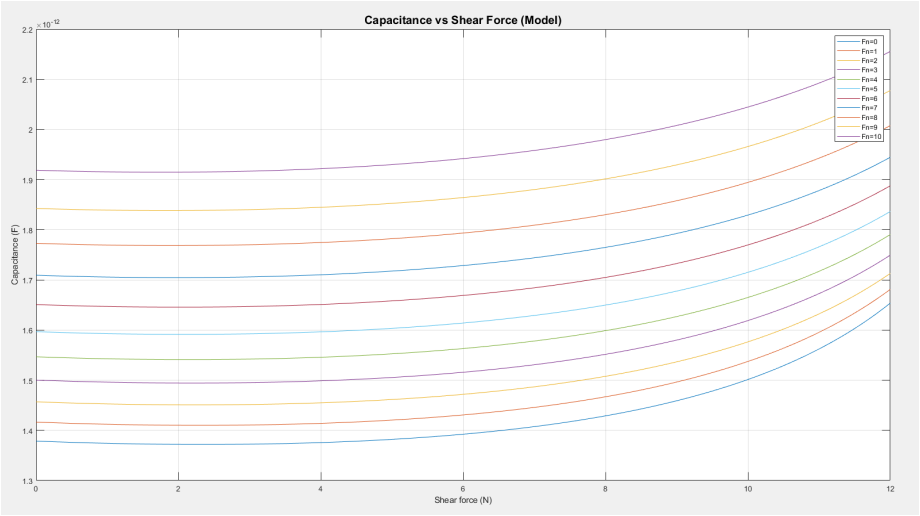

Figure 7.3: The capacitance modeled over an increasing shear force with different normal forces acting on it.

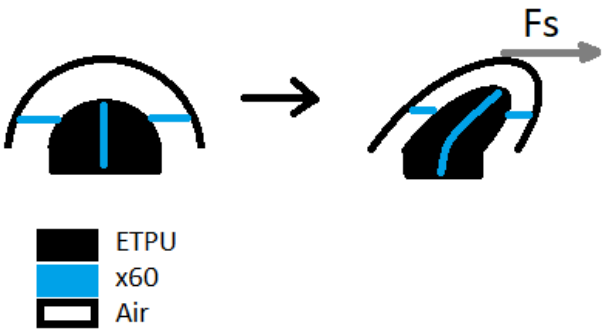

Figure 7.4: Deformation of the cylindrical structure caused by shear force.

Chapter 8

Conclusions

The main goal was to determine if 3D-printed structures, consisting of carbon doped thermoplastics (ETPU), can be used for sensing shear forces. Two designs were chosen: the three layered structure and the cylindrical structure. Both designs are analytically and physically investigated to determine if the structures are feasible for shear force sensing.

The three layered structure showed promising results. The designed model related to the physically measured values for forces between two and twelve Newtons and showed the same behavior, making it possible to further design new sensors with this model and predict their behaviour. The capacitance gain was non linear, however it did correspond to the measured gain.

The cylindrical structure did not correspond with the model, mostly because of the deformation that happened to the cylinders. This deformation made the cylinders not behave as expected when designing the model and made the model unusable in this particular situation. The model for the cylindrical structure could be more useful if a stiffer conductive filament was used. There was a change in capacitance corresponding to the shear force ranging from one to twelve Newton, however this could not be predicted with the determined model

Both sensors have their own way of reacting to an applied shear force. The three layered sensor has a non linear capacitance increase whereas the cylindrical has a more linear increase in capacitance.

However, both structures are capable of detecting shear forces. The three layered sensor can detect shear forces in a range of two to twelve Newton leading to a change in capacitance between 5.7 pF and 6 pF. The cylindrical sensor was able to detect shear forces from one newton to twelve newton for both sides of the inner cylinder. Leading to a change in capacitance between 10 pF and 110 pF for the inner cylinder side experiencing a decrease in distance to the shell. The other side showed a change in capacitance between 10 pF and 14.5 pF.

Bibliography

[1] F. Nadin, "When is 3d printing the best solution for production?" approached on 2018-12-27. [Online]. Available: https://www.sculpteo.com/blog/2016/05/25/when-is-3d-printing-the-best-solution-for-production/

[2] M. Welleweerd, "3d printing a three degrees of freedom force sensor," MSc report, UTwente, RaM, 2017.

[3] E. Perez Lorea, "3d printed sensor to detect muscle contraction by means of force myography," MSc Report, UTwente, RaM, 2017.

[4] J. Tichelaar, "3d-printed implementation of a tactile pressure sensor working in multiple dof," BSc Report, UTwente, RaM, 2018.

[5] B. Eijking, "Tactile whisker sensor using flexible 3d printed transducers," BSc Report, UTwente, RaM, 2017.

[6] G. Wolterink, R. Sanders, and G. Krijnen, "Thin, flexible, capacitive force sensors based on anisotropy in 3d-printed structures," in *2018 IEEE SENSORS*, 10 2018, pp. 1–4. [Online]. Available: https://doi.org/10.1109/ICSENS.2018.8589584

[7] D. Wang, "What are you sensing? capacitive sensing for proximity detection and more," approached on 2019-1-3. [Online]. Available: https://e2e.ti.com/blogs_/b/analogwire/archive/2014/12/05/what-are-you-sensing-capacitive-sensing-for-proximity-detection-and-more

[8] C. Shemelya, L. Banuelos-Chacon, A. Melendez, C. Kief, D. Espalin, R. Wicker, G. Krijnen, and E. MacDonald, "Multi-functional 3d printed and embedded sensors for satellite qualification structures," in *2015 IEEE SENSORS*, Nov 2015, pp. 1–4. [Online]. Available: https://doi.org/10.1109/ICSENS.2015.7370541

[9] S. Toyama, "Development of wearable sheet-type shear force sensor and measurement system that is insusceptible to temperature and pressure," *Sensors (Basel, Switzerland)*, 2017. [Online]. Available: https://dx.doi.org/10.3390%2Fs17081752

[10] H. Qi and M. Boyce, "Stress-strain behavior of thermoplastic polyurethanes," *Mechanics of Materials*, vol. 37, pp. 817–839, 08 2005. [Online]. Available: https://doi.org/10.1016/j.mechmat.2004.08.001

[11] Wikipedia, "Poisson's ratio," approached on 2019-1-9. [Online]. Available: https://en.wikipedia.org/wiki/Poisson%27s_ratio

[12] A. Kalaiarasi, "Design modeling and analysis of cantilever based mems devices with improved performance," Ph.D. Thesis, Anna University, 2014.

[13] H. B. Palmer, "The capacitance of a parallel-plate capacitor by the schwartz-christoffel transformation," *American Institute of Electrical Engineers, Transactions of the*, vol. 56, pp. 363 – 366, 04 1937. [Online]. Available: https://doi.org/10.1109/T-AIEE.1937.5057547

[14] V. Leus and D. Elata, "Fringing field effect in electrostatic actuators," TECHNION— Israel Institute of Technology, Tech. Rep., 01 2004.

[15] H. Yang, "Microgyroscope and microdynamics," Ph.D. Dissertation, 2000.

[16] Flashforge, "Flashforge creator pro 3d printer," approached on 2019-1-21. [Online]. Available: http://www.flashforge.com/creator-pro-3d-printer/

[17] 3DHubs, "Introduction to fdm 3d-printing," approached on 2019-1-21. [Online]. Available: https://www.3dhubs.com/knowledge-base/introduction-fdm-3d-printing

[18] D. Engineering, "Flexion extruder," approached on 2019-1-21. [Online]. Available: https://flexionextruder.com/

[19] ETPU, "Pi-etpu 95-250 carbon black," approached on 2018-11-23. [Online]. Available: https://rubber3dprinting.com/pi-etpu-95-250-carbon-black/

[20] NinjaFlex, "Ninjaflex," approached on 2018-11-24. [Online]. Available: https://ninjatek.com/ninjaflex/

[21] Flexion, "X60," approached on 2018-12-27. [Online]. Available: https://flexionextruder.com/shop/x60-ultra-flexible-filament-black/

[22] H. Packard, *HP 4284A PRECISION LCR METER OPERATION MANUAL. 6th ed.*

[23] Autodesk, "Fusion 360," approached on 2019-1-21. [Online]. Available: https://www.autodesk.com/products/fusion-360/overview

[24] Simplify3D, "Simplify3d," approached on 2019-1-21. [Online]. Available: https://www.simplify3d.com/

[25] K. Wang, *Die Swell of Complex Polymeric Systems*. IntechOpen, 2012. [Online]. Available: http://dx.doi.org/10.5772/50137

[26] S. Corporation, "Smac mca lca series," approached on 2019-1-22. [Online]. Available: https://www.smac-mca.com/lca-series-p-15.html

[27] Mathworks, "Matlab," approached on 2019-1-22. [Online]. Available: https://www.mathworks.com/products/matlab.html

[28] M. Schouten, R. Sanders, and G. Krijnen, "3d printed flexible capacitive force sensor with a simple micro-controller based readout," in *2017 IEEE SENSORS*, Oct 2017, pp. 1–3. [Online]. Available: https://doi.org/10.1109/ICSENS.2017.8233949

Appendix A

Printed supports

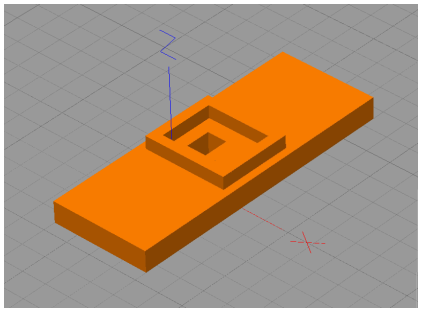

(a) Slicer model of the sensor holder

(b) Printed sensor holder, after use

Figure A.1: Sensor holder design and print

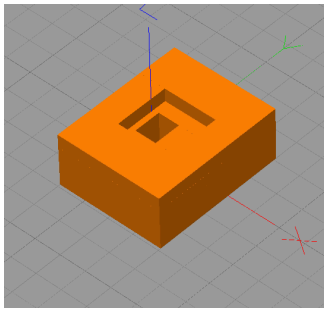

(a) Slicer model

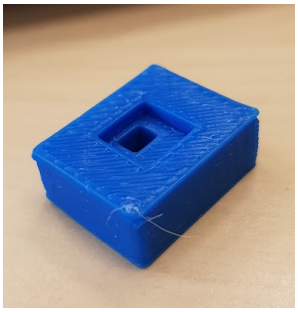

(b) Printed model

Figure A.2: Holder for the top layer of the three layered sensor designed in Simplify3D and 3D-printed using ABS plastic filament.

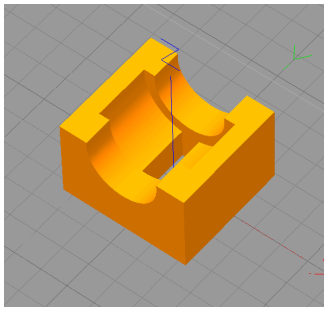

(a) Slicer model

(b) Printed model

Figure A.3: Holder for the top layer of the cylindrical sensor designed in Simplify3D and 3D-printed using ABS plastic filament.

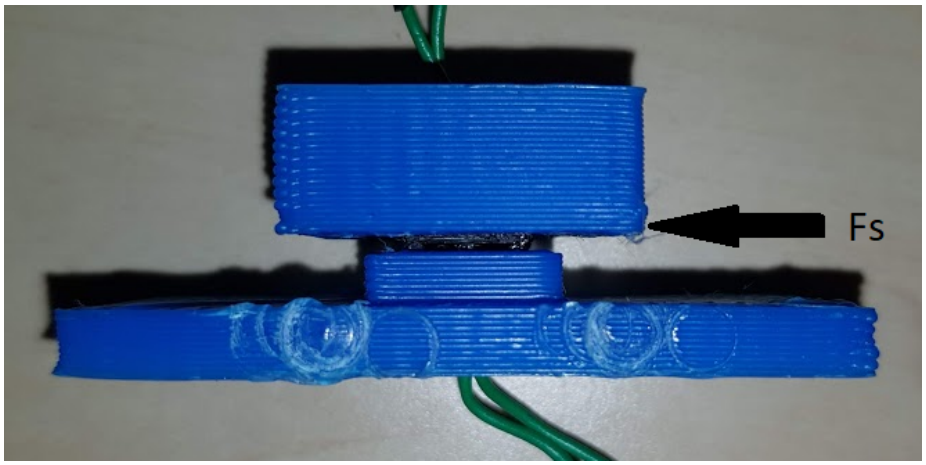

Figure A.4: The application of horizontal force is shown using both the bottom and top layer holders.

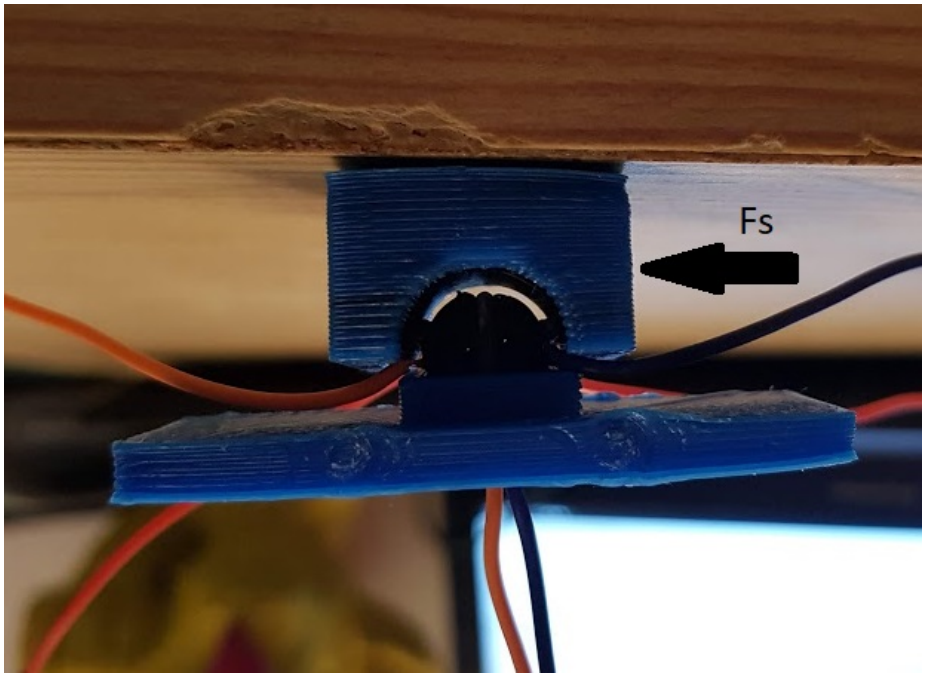

Figure A.5: The application of horizontal force is shown using both the bottom and top cylinder holders.